CHALMERS
UNIVERSITY OF TECHNOLOGY

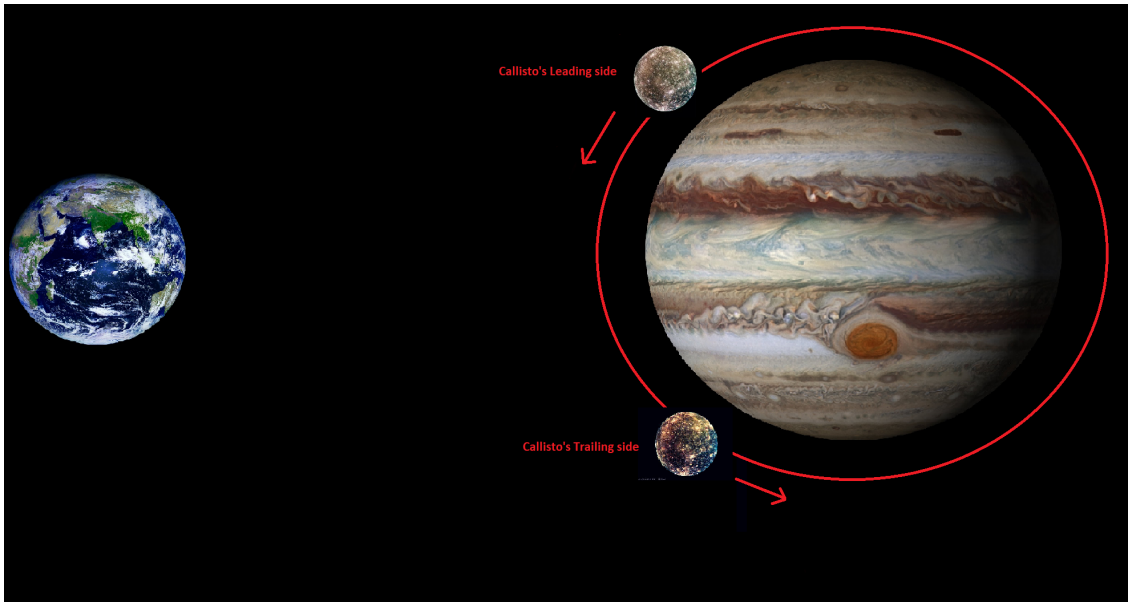

Constraints on the CO content of Callisto's exosphere based on ALMA archival data

Master's thesis in Physics and Astronomy

NEGAR ENTEKHABI

Department of Space, Earth and Environment
CHALMERS UNIVERSITY OF TECHNOLOGY
Gothenburg, Sweden 2018

Master's thesis 2018

Constraints on the CO content of Callisto's exosphere based on ALMA archival data

NEGAR ENTEKHABI

CHALMERS
UNIVERSITY OF TECHNOLOGY

Department of Space, Earth and Environment
Radio Astronomy and Astrophysics
Onsala Space Observatory
Chalmers University of Technology
Gothenburg, Sweden 2018

Constraints on the CO content of Callisto's exosphere based on ALMA archival data

Supervisors: Dr.Eva Wirström, Dr.Sebastien Muller
Examiner: Prof.Wouter Vlemmings

Master's Thesis 2018
Department of Space, Earth and Environment
Chalmers University of Technology
SE-412 96 Gothenburg
Telephone +46 31 772 1000

Onsala Space Observatory
SE-439 92 Onsala, Sweden
+46 31-772 5500

Cover: When Callisto is moving towards the Earth, the hemisphere of Callisto which is facing the Earth is leading hemisphere and when it is receding, its trailing side is being observed from the Earth.

Typeset in LaTeX
Gothenburg, Sweden 2018

Abstract

Callisto is the second largest moon of Jupiter and the third largest in the Solar System and in a wide enough orbit to avoid Jupiter's harmful magnetosphere. It is tidally locked in its orbit so that the same side of Callisto always looks at Jupiter. Water (H_2O) detections from the two leading and trailing hemispheres of Callisto are somewhat different which might be an indication of asymmetry in its atmosphere.
A theoretical atmosphere density model of Callisto predicts that if the atmosphere of Callisto has been formed in oxidizing state, the top constituents of sublimation profile density are expected to be H_2O, CO and CO_2. Callisto's tenuous CO_2 atmosphere have been observed directly by the Galileo Near Infrared Mapping Spectrometer. Likewise, water absorption lines are detected from the leading hemisphere of Callisto. These findings and lack of information about CO, motivated us to search for CO lines in Callisto's atmosphere. ESA's (European Space Agency) JUICE spacecraft in 2030 will investigate Callisto's exosphere in more detail. To prepare for that investigation it might be possible to use ground-based data from Atacama Large Millimeter Array (ALMA) in Chile to detect carbon monoxide (CO) lines.
All available observations covering the $CO_{J=2-1}$ transition frequency toward Callisto are extracted from ALMA archive. Then, to find the best fitted visibilities, the extracted data are analysed using a circular disc model for Callisto and spectra are extracted directly from the interferometric visibilities.
Afterwards, averaging of the fitted spectra are performed for both leading and trailing hemispheres. Since the average spectra does not show any emission or absorption CO line, upper column density of CO by using rms noise level is calculated which gives $\sim 2 \times 10^{15}$ cm^{-2}. The result shows that, CO is likely not the most dominant species in Callisto's atmosphere.
For comparison, $CO_{J=2-1}$ spectra towards Saturn's moon Titan, are also extracted from the ALMA archive. The detected lines are strong and broad and CO column density is estimated to be at least five to six orders of magnitude higher in the atmosphere of Titan, than in that of Callisto.

Keywords: Callisto, Atmosphere, CO, ALMA

Contents

List of Figures

List of Tables

1
Introduction

1.1 Planetary Atmospheres

All of the planets in the solar system and some of the smaller bodies (moons) as well, have an outer layer of gas called an atmosphere which is kept in its place due to the pull of the gravity of that body and can extend thousands of kilometers into space. The atmospheres of celestial bodies protect them from ultra-violet radiation and regulate the temperature difference between day and night. Atmospheres are defined by their density, temperature, pressure and chemical composition and they differ from one case to another. Because the celestial bodies have various and different structure and they are located at different distances from central star or planet.
As an example, the atmosphere of the Earth is mostly composed of nitrogen ($\sim 78\%$), oxygen ($\sim 20\%$) and trace amount of carbon dioxide, while nearby Venus has a thick carbon-dioxide atmosphere and the giant outer planets have extremely thick atmospheres of hydrogen and helium.
Studying the composition of the atmosphere of a celestial object, reveals the history about either its evolution or the formation of planets and planetary disk. For example, hydrogen and hydrogen rich molecules are dominant elements in the outer parts of the Solar System. This fact implies that, at the early stages of the formation of the planetary disk of the Solar System, the light gas (hydrogen and helium) were blown away from the Sun, via the radiation pressure and the solar winds. On the other hand, knowing the evolution of the Earth makes it possible to gain knowledge about either what primary conditions are needed or, how long it takes for a planet or moon to be habitable.

1.2 Callisto

The Galilean moons are the four largest moons of Jupiter which are named Io, Europa, Ganymede and Callisto, in order of increasing distance to Jupiter. Callisto is the second largest moon of Jupiter and the third largest in the Solar System. It is about the same size as Mercury but has only a third of its mass. Callisto is the only Galilean moon far enough out from Jupiter's strong magnetosphere that it does not experience harmful radiation.
Callisto has low albedo[1] and generally is a dark object, though its leading hemisphere is even darker and redder than trailing side (Moore et al.,2004).

[1] Albedo is a dimensionless quantity to measure the part of solar radiation which is reflected by a planet or moon.

Callisto has an ancient cratered surface, indicating that geological processes have not been active for billions of years. In fact in the Solar System, Callisto is the only celestial object with diameter larger than 1000 km which has not revealed any indication of experiencing resurfacing, since collisions have formed its surface (NASA,2017b). However, it may hold an underground ocean which leads to be thought that it could shelter an extraterrestrial life (Khurana et al.,1998) (Showman and Malhotra,1999) (Sohl,2009).
Arguments for an ocean mainly come from two pieces of evidence. The first argument came to light when scientists detected regular fluctuations of Callisto's magnetic field, as the moon revolved around Jupiter. It implies that there are electrical currents within the moon, agitated by the planet's magnetic field. since salt water is a great conductor of electricity and Callisto has a rocky surface and a thin atmosphere, a likely explanation of the current would be a salty ocean under the moon's surface (Zimmer et al.,2000).
The second reason is based on that, Callisto is not in an orbital resonance and thus, is not tidally heated (Musotto et al.,2002). Also, it has been thought that Callisto has been formed through gradual accretion from the planetary disk of gas and dust, that surrounded Jupiter after its formation (Canup and Ward,2002). Therefore, Callisto's slow accretion and lack of tidal heating, mean that there were not enough time for differentiation. Most likely, one of the most basic reasons of the formation of a subsurface salty ocean is the slow convection in the interior of Callisto.

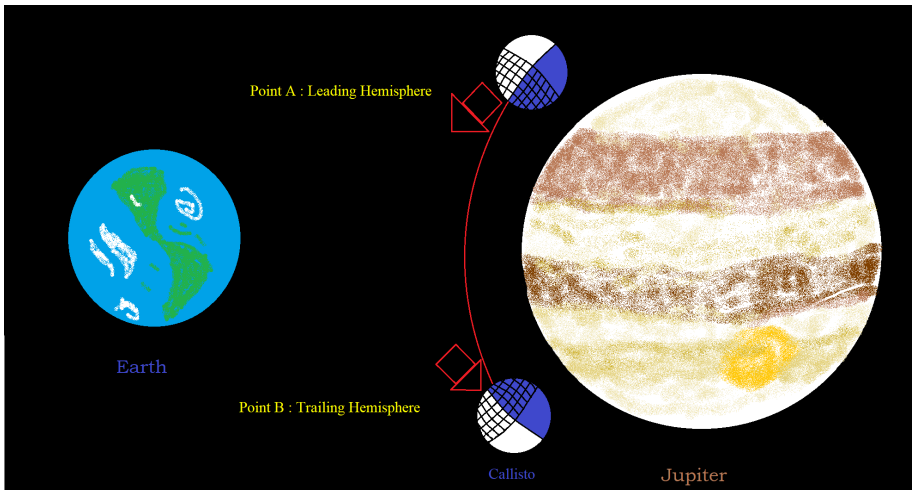

Figure 1.1: Callisto is tidally locked so that the same hemisphere of Callisto (blue division), is always looking at Jupiter. At point A which Callisto moves towards the Earth, the checkered side of Callisto is leading side and at point B in which Callisto recedes, the checkered side is the trailing hemisphere of Callisto.

Callisto, like the Moon of the Earth, is tidally locked in its orbit around Jupiter, so that the same hemisphere always looks at Jupiter (Blue side of Callisto, Fig 1.1). When Callisto moves towards the Earth, the leading hemisphere of Callisto faces the Earth (Checkered side at point A, Fig 1.1), while its trailing hemisphere faces the Earth when Callisto moves away (Checkered side at point B, Fig 1.1). It is noteworthy that, water measurements from the two hemispheres of Callisto are

different and it shows an asymmetry between two sides of Callisto (Hartogh et al., 2013). Hence, the hemisphere of Callisto must be determined for each observation. It can be distinguished by checking Callisto's relative motion with respect to the Earth at the date of observation, at NASA Jet Propulsion Laboratory horizons web-interface[2].

Callisto has a very tenuous carbon dioxide (CO_2) atmosphere which has been observed directly by the Galileo Near Infrared Mapping Spectrometer, with a column density approximately equal to 9.2×10^{14} cm^{-2} (Carlson,1999). In fact, the atmosphere of Callisto is so thin that molecules collide with each other rarely and consequently they don't participate in chemical reactions. Such a thin atmosphere can be easily annihilated due to the ultra-violet radiation of the Sun. This radiation breaks the molecules into ions and electrons and then, these charged particles are moved away by Jupiter's magnetic field. If this weak atmosphere exists, it means there must be a steady flux of carbon dioxide molecules into the atmosphere of Callisto. Emitting CO_2 from the surface of Callisto is the most probable alternative of CO_2 steady flux. Because images from the surface of Callisto show some erosion that can be the result of carbon dioxide outgassing (Carlson,1999).

Photoionization is a process in which atoms or molecules are ionized by electromagnetic radiation. Simulation of high electron density in the atmosphere of Callisto concludes that, photoionization of observed CO_2 molecules in the atmosphere of Callisto, can not generate such high electron density. Indeed, Callisto's atmosphere must be $20 - 100$ times denser than the measured CO_2 density to obtain that result (Kliore et al.,2002).

Observations from Callisto's leading hemisphere by using high far ultra-violate sensitivity of Hubble Space Telescope, showed different strength atomic oxygen emissions. The ratio of these lines is consistent with dissociative excitation of O_2. It suggests that, molecular oxygen with $\sim 4 \times 10^{15}$ cm^{-2} column density rather than other possible oxygen bearing molecules, is the second major molecule in the atmosphere of Callisto (Cunningham et al.,2015). The calculated column density of O_2 implies that, Callisto's atmosphere is collisional rather than collision-less. But since O_2 has not been observed directly, this assumption is not considered.

As it is mentioned, Callisto is not fully differentiated and its surface is assumed to consist of about the same portion of ice and non-ice (rock) material (Nagel et al.,2004). A flux of particles from Callisto's surface, is the reason of its atmosphere existence. Sublimation, ion-sputtering and photon-stimulated desorption are the processes thereby particles from Callisto's surface are separated and travel their free trajectories up to the atmosphere. In a recently published theoretical atmosphere model, using a Monte-Carlo approach (Vorburger et al.,2015), Callisto's atmosphere density is calculated based on its ice and non-ice surface.

For the ice composition, two scenarios are considered. The first one is oxidizing state which represents that the satellite is formed in proto-solar nebula, at the same time of giant planet formation. The second outline is reducing state which demonstrates that the satellite is formed in Jovian sub-nebula. For non-ice component, the composition of two types of chondrites are implemented.

The density profile of sublimated particles from Callisto's icy surface at the sub-solar

[2]https://ssd.jpl.nasa.gov/horizons.cgi

point shows that, top three density profiles belong to H_2O, CO and CO_2, in order of decreasing density (Fig 1.2, left panel). Density profile of sputtered particles from Callisto's icy surface at the sub-solar point, as well as from the night side, also confirms the existence of H_2O, CO and CO_2, but in higher altitudes and with lower densities (Fig 1.2, right panel). Comparing the density profiles of sublimated and sputtering particles from icy surface in the model of oxidizing state, shows that the sublimated particles dominate close to Callisto's surface, though their density profiles decrease much more rapidly with altitude, than the sputtered particles.

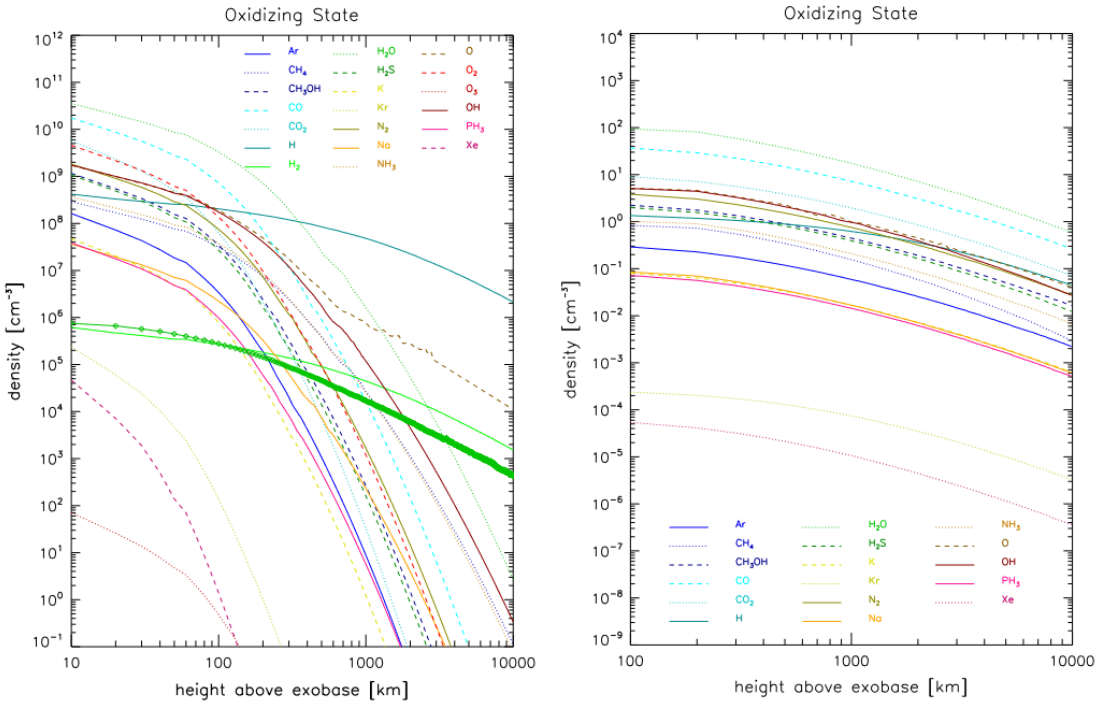

Figure 1.2: Density profiles of particles that have been sublimated and sputtered from Callisto's icy surface. The left panel shows the result of sublimated particles and the right panel shows the results of sputtered particles. Both diagrams are the results of the assumption of oxidizing state (Vorburger et al.,2015).

Referring to CO_2 and H_2O observations in the atmosphere of Callisto and the results of the theoretical atmosphere model, which predicts that the most dominant molecules in Callisto's atmosphere are expected to be H_2O, CO and CO_2, it becomes clear why we were motivated to search for CO and why we expect to be able to see CO lines in the atmosphere of Callisto.

1.3 Titan

Titan is the largest moon of Saturn and is the second largest in the Solar System, after Jupiter's moon Ganymede. Titan is the only moon in the Solar System with a dense atmosphere like the Earth, predominantly made up of nitrogen and other compounds commonly associated with life. It is the only object rather than the Earth,

on which surface liquids such as lakes, rivers and seas has been observed by Cassini, an unmanned spacecraft sent to the planet Saturn (Coustenis and Hirtzig,2009). Titan's surface water because of its low surface temperature (94 K) is frozen and liquid methane and ethane rather than water dominate the surface liquids of Titan (Mitchell et al.,2015). However, it has an under ground water ocean containing a high density of dissolved salts (Fortes,2000)(Mitri et al.,2014).
Mass spectroscopy of NASA's Cassini probe inferred the existence of molecule vinyl cyanide (C_2H_3CN or CH_2CHCN) in Titan's atmosphere, as the best candidate molecule to form cell membranes (Stevenson et al.,2015). The findings were just a simulation until NASA researchers by using archival data of Atacama Large Millimeter Array (ALMA), detected a large amount of vinyl cyanide in the upper atmosphere of Titan. Just like this thesis in which, ALMA archival data is used to search for spectra in the frequency range in the vicinity of CO_{2-1} transition, three strong rotational lines of vinyl cyanide, originated mostly at altitude above 200 km, in the range of 230 to 232 GHz were detected by ALMA data. According to the best fitting model, the vertical column density of vinyl cyanide lies in the interval of $3.7 \times 10^{13} - 1.4 \times 10^{14}$ cm^{-2} (Palmer et al.,2017).
The direct evidence of the presence of vinyl cyanide in the atmosphere of Titan and considering the fact that, a rain of particles transports the molecules formed in the upper atmosphere down to the surface (Raulin and Owen,2003), leads to estimate the amount of C_2H_3CN in Ligeia Mare, Titan's second largest lake (Wasiak et al.,2013). Using the ratio of vinyl cyanide production and assuming that the relation between production and saturation rate of vinyl cyanide is linear, implies vinyl cyanide exists in the range of $\sim 10^{13} - 10^{15}$kg in Ligeia Mare. This amount of vinyl cyanide can form $\sim 10^7$ cell membranes per cubic meter in this sea (Palmer et al.,2017).

1.4 ALMA

Most of physical processes and objects in the universe emit electromagnetic radiation which reveals some of their properties. Electromagnetic radiation is the main source of astronomical information and extends from short wavelengths such as gamma and X-rays, passing through visible light to the long wavelengths like radio waves.
Radiation with higher frequencies are blocked by the Earth's atmosphere. So, to detect ultraviolet or X-ray radiation, a telescope above the Earth's atmosphere is needed. Optical telescope is used to receive visible light from astronomical sources and unlike the mentioned case, it is possible to use the ground based telescopes. But since the light rays while passing through the air are perturbed, the result will be a blurred image. Consequently, only a telescope above the Earth's atmosphere may achieve much sharper images which is the reason of why the Hubble Space Telescope (HST) has been built (Choudhuri,2014).
Radio astronomy use radio telescopes to receive radio signals from astronomical sources. A radio telescope is made up of an antenna and a receiver. The antenna concentrates the radio waves at the focal point and the receiver converts the signals to a measurable voltage. Since the atmosphere of the Earth does not affect on radio waves with longer wavelengths (> 10 cm), the resolution of the ground based radio telescopes is not limited by atmospheric turbulence. But, while detecting

radio waves with shorter wavelengths, the results of atmospheric turbulence leads to obtain lower resolution. If the signals of single radio telescopes which are arranged as an array to observe a body simultaneously, are combined, it will be called a radio interferometer and the final image resolution will be higher than a single radio telescope.
Radiation with short wavelength (higher frequency) generally comes from more energetic processes in the universe such as explosion of stars or galaxies, Supernovae and very hot stars, whereas radiation with longer wavelength (lower frequency) in millimeter and sub-millimeter range, is emitted from relatively cold objects like planets and satellites. Dense molecular gas cloud from which stars are born and planetary disc is formed, cosmic microwave background (CMB) and the emitted radiation of rotational transitions of molecules are other examples of long wavelength radiation. Studying this kind of radiation which occurs even in cold interstellar gas, reveals some facts about the physical condition in which the molecules exist.
The Atacama Large Millimeter/sub-millimeter Array (ALMA) is an astronomical interferometer of radio telescopes in Atacama desert of northern Chile. It is the most powerful observatory in studying the universe at millimeter and sub-millimeter wavelengths and the largest and the most expensive ground based observatory. It's designed in particular to observe the cool universe, but can observe a large range of astronomical sources, from comets to planets and their satellites in the Solar System to the most distant galaxies in the universe.
ALMA consists of 66 radio antennas, with 12 meter (54) and 7 (12) meter in diameter. These antennas are transportable and they can be moved across the desert from 150 meters to 16 kilometers by special trucks, without damaging their performance. The signals of radio antennas are combined to perform as an interferometer which can be assumed as a single giant telescope, with the aperture as large as the maximum separation between telescopes. This combination allows astronomers to have an image of an object with very finest details and higher resolution.
The angular resolution of a single radio telescope is defined as:

$$R = \frac{\lambda}{D} \tag{1.1}$$

In which R is in radians, λ is the observed wavelength (m) and D is the diameter of the telescope (m). According to this relation, the angular resolution of a telescope will be high, either if its diameter would be large or the observed wavelength would be short. In the case of an interferometer, the resolution is defined as:

$$R = \frac{\lambda}{B} \tag{1.2}$$

In which B is the maximum separation between radio telescopes of an array and is called baseline. Larger baseline leads to achieve higher resolution.
Because of the effects of atmospheric water vapors on the radiation (in millimeter/sub-millimeter wavelength) coming from space, building ALMA observatory in the middle of the driest desert on the Earth, high altitude (5,050 meters above sea level) and faraway from radio interference due to man-made noises, made it to be the best

place for observations[3]. Furthermore, the center of the galaxy which is located in southern sky, is observable by ALMA.
One of the most important factors of a radio antenna, is the surface accuracy of its aperture. To prevent losing partial radiation and gain a good image of the target source, it needs to be better than a few percent of observing wavelength (better than $\sim \lambda/20$). ALMA is made of very accurate and smooth dishes and the surface of the most dishes of ALMA, are made of ultra stable carbon fiber reinforced plastic. Also, the antennas are made so that they can survive of the harsh environmental conditions like strong winds, intense sunlight and temperature variation.
While observing a target on the sky, the final detected signal is mixed with some noise which comes from the sky or electrical devices. The radiometer formula describes the rms noise of an observation (Wilson et al.,2013):

$$\Delta T_{rms} = T_{sys} \frac{1}{\sqrt{\Delta \nu t}} \tag{1.3}$$

In which ΔT_{rms} is the resulting rms noise, T_{sys} is the noise of the receiver and is described by the system temperature, $\Delta \nu$ is the bandwidth and t is the integration time. Since the thermal noise of the system is the most important factor to increase or decrease the rms noise, ALMA's electronic devices are kept at a chilly 4 Kelvin (-269 C°).
The produced data with ALMA for each observation are saved in an archive. After the observation and calibration and a propriety period of time, the data become public and they can be available through an online archive query. Since Callisto is commonly used as a calibrator source for ALMA observations, this archive has been used to extract available Callisto data for the purpose of this thesis.
When searching for a specific line at a specific frequency, two main factors must be considered. At the first, one needs to look for a band of frequency to be able to pick up the target line. Additionally, to be able to observe the main line, defining the accurate spectral resolution is required. These parameters plus some extra components, like integration time could be determined for each specific project at the first page of ALMA online archive. These capabilities, make ALMA online archive to be the best data source for researchers, to have access easily and fast to the related data.

[3]http://www.almaobservatory.org/en/about-alma-at-first-glance/privileged-location/

2
Theory

2.1 Interferometry

Two main features of a radio telescope are a large radio antenna and a radio receiver which respectively, are used to collect radio waves coming from celestial sources and convert the energy of electromagnetic radiation to the measurable voltage. As it is mentioned, the resolving power of a single dish is limited due to its diameter. The larger the aperture diameter, the higher resolution will be achieved. But since it is prohibitive and physically impossible to build a telescope with the aperture of extremely large diameter, interferometry solves this problem, partly.
Interferometers are made up of two or more single radio antennas to collect the radio waves and then, by merging these observations one can achieve an interference pattern (that is why it is called Interferometry). In a simple word, one can assume that two radio antennas which are settled with a distance between them which is called baseline, is an interferometer with the diameter equal to the baseline. The shortest diameter of an interferometer is when two radio antennas are exactly next to each other.
If the target source in the sky is located within x and y coordinate plane, the projected baselines of the array of an interferometer are in u and v coordinate plane which are called spatial frequencies. An interferometer measures the interference pattern created by its array in the u-v plane. The response of an interferometer is a complex quantity called visibility which consists of discrete components of observed brightness distribution on the sky. The Fourier transform is a mathematical tool which is used in interferometry, relating the measured visibility (V(u,v)) to the intensity (I(x,y)) of the source in the sky. The Fourier transform of a function $f(x)$ is defined as :

$$F[f(\vec{x})] = G(\vec{\nu}) = \int f(\vec{x}) \times exp(-2\pi j \vec{\nu}\vec{x}) d\vec{x} \tag{2.1}$$

According to this relation, a FT rewrites a function into its reciprocal space, from time to frequency or from space to spatial frequency. FT keeps the information encoded in the function and expresses it just in different basis.
An interferometer with two radio telescopes provides very limited information about the source, because they do not cover all the spatial frequencies of the target source. One of the solution to achieve more coverage, is to move telescopes to change the baseline spacing or locate a number of telescopes along the baseline and repeat the observation.

Most of the astronomical radio sources are stationary and they are virtually the same over long periods of time. Therefore, another solution to gain much more coverage of u-v plane, is to use Earth rotation. When the Earth rotates, the position of the telescopes follows a trajectory along a section of an ellipse, as seen from the source. As the observation proceeds, the position of the telescopes travels a large part of the elliptical path and consequently fills in u-v plane, much more than before. This is called Aperture Synthesis which is shown in figure 2.1.

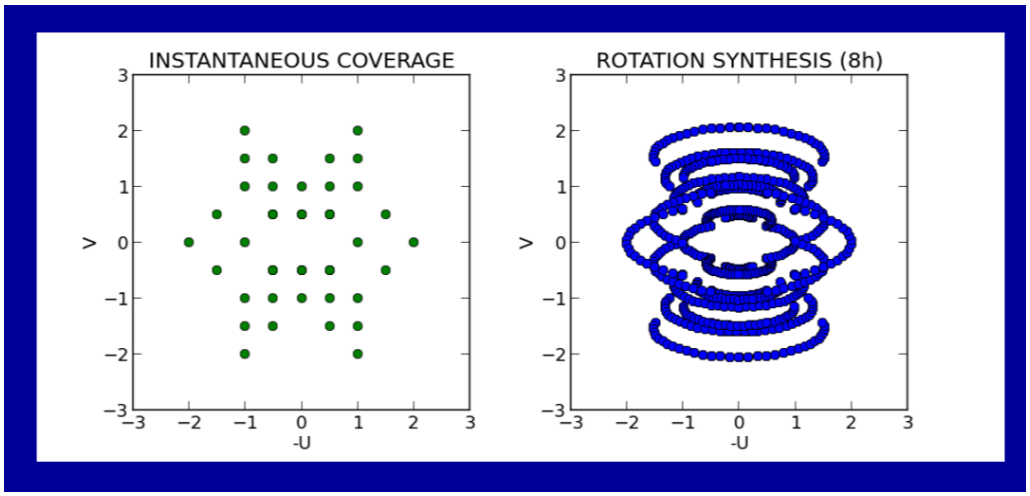

Figure 2.1: U-V coverage and Aperture Synthesis.

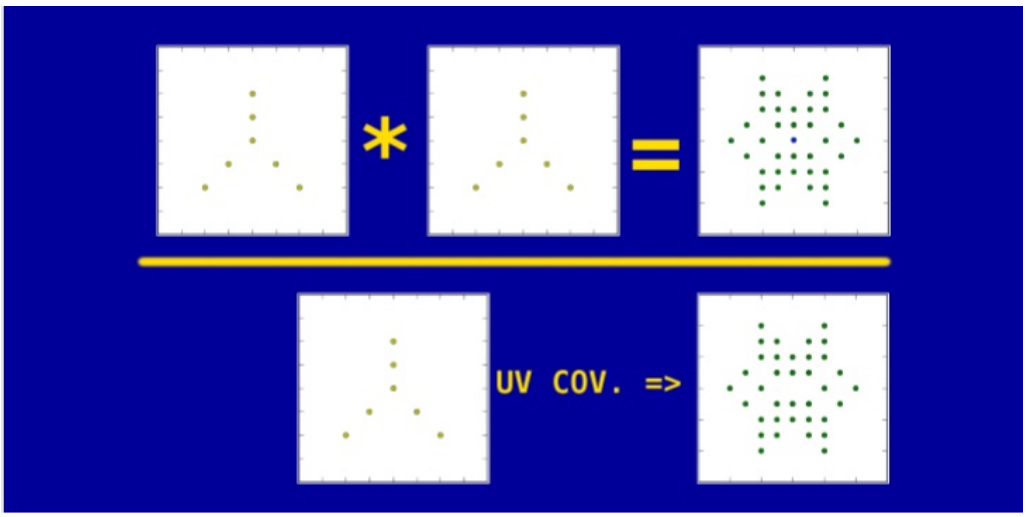

Figure 2.2: Auto-correlation of the array and UV coverage without zero spacing term.

Two other concepts which are required to be introduced are, Convolution and Cross-correlation. The convolution ($\star$) of two functions f and g is a shift-multiply-integrate operator:

$$[f \star g](\vec{\tau}) = \int_{-\infty}^{\infty} f(\vec{x}) \times g(\vec{\tau} - \vec{x}) d\vec{x} \tag{2.2}$$

And cross-correlation of two functions f and g is given by:

$$[f * g](\vec{\tau}) = \int_{-\infty}^{\infty} f^*(\vec{x}) \times g(\vec{x} + \vec{\tau}) d\vec{x} \tag{2.3}$$

Given two functions f and g, the FT of their convolution is equal to the product of their FT. It means multiplying in Fourier space is equivalent to convolving in ordinary space:

$$F[f \star g] = F[f] \times F[g] \tag{2.4}$$

The aperture of an interferometer is the pairs of telescopes which are separated by baselines. Auto-correlation of the array configuration (upper image in figure 2.2) without zero spacing term (lower image in figure 2.2), gives the UV coverage of the baselines as seen from the source .
While observing with an optical telescope, due to diffraction the image of a point source will be a blurry shape surrounded by a series of bright rings called Point Spread Function (PSF). PSF of an interferometer equals the FT of the aperture's auto-correlation in which, the zero-spacing term (0,0) has been removed, because the shortest baseline of an interferometer never becomes zero. It must be noted that (0,0) spatial frequency in u-v coordinate is very important and it contains total flux of visibility of the source which can not be measured by interferometry. Lack of measurements of short spatial frequencies, leads to get large gap around (0,0) in u-v plane and consequently much information about the source will be lost. Therefore, to prevent of losing more data while observing extended sources[1], shorter baselines must be used.

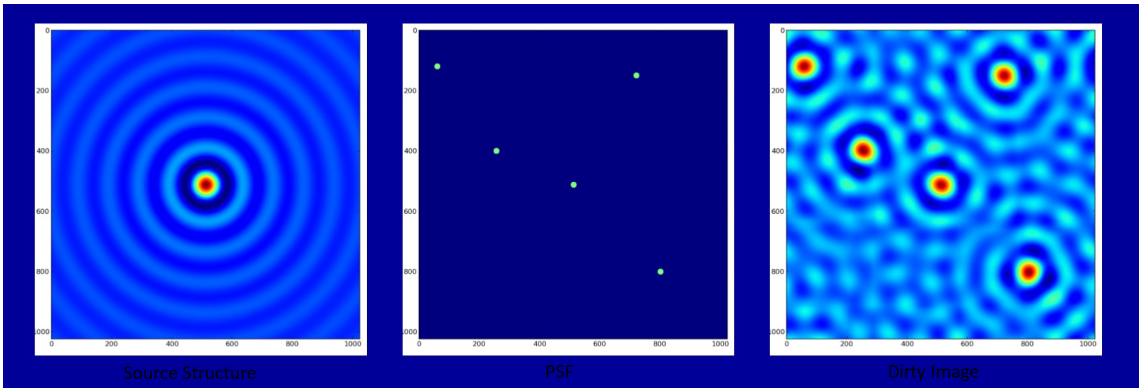

Figure 2.3: Convolution of PSF and target source resulting in Dirty Image.

While observing a source with a generic structure, the obtained image is the Convolution of the source structure with PSF (dirty beam). In Figure 2.3, the first image in the left side is PSF, the second one in the middle is the real source structure and the last one is the convolution of PSF and the source structure which is the result of observation and is also called Dirty Image. To achieve a better and smaller PSF which leads to have an image with higher resolution, the diameter of the aperture

[1] An extended source when observed with an interferometer, is a source such as galaxies whose angular size is greater then the λ/B_{min} angular resolution, given by the shortest baseline B_{min}.

which is equivalent to the baselines in interferometers, must be larger. Using deconvolution method to clean the dirty beam from dirty image, the structure of the source will be extracted.

2.2 Transition Frequency

In order to explain the data analysis, some spectroscopy theory has to be introduced. Spectroscopy is used to study the electromagnetic radiation emitted by atoms, ions or molecules. The properties of radiation (frequency, intensity, polarisation) reveals much information about the composition, density, temperature, etc. of the celestial object from which radiation come from.
According to the quantum mechanics, when a transition between different energy levels of an atom, ion or molecule occurs, a radiation with specific frequency is emitted. Atoms and ions contain just electronic states and their transitions involve electrons. While in molecules, there are three types of energy levels: Electronic states, vibrational states and rotational states. Molecules can vibrate through quantized vibrational levels within electronic states and within vibrational levels, molecules can rotate through quantized rotational levels, as well. The point of this project is to consider the rotational line of CO for $J = 2-1$ transition, with related frequency ν_{2-1}=230.538 GHz (Phillips et al.,1973).
Carbon Monoxide CO, is an asymmetric molecule which has a non zero electric dipole moment. Existence of electric dipole moment is the result of significantly asymmetric charge distribution. Electric dipole moment is the difference between positive and negative charges within the whole molecule and most commonly expressed in Debye[2]. Polar molecules like CO radiate with specific frequency at each of their rotational transition. To obtain the corresponding frequency, first of all angular momentum L of a molecule, is defined:

$$L = n\hbar \tag{2.5}$$

Where n is the principle quantum number (n=1, 2, 3, ...) and $\hbar$ is the reduced Planck constant ($\hbar = \frac{h}{2\pi}$). Planck constant is denoted by h and equals to $\sim 6.63 \times 10^{-34}$ m^2 kg s^{-1}. The rotational kinetic energy E_{rot} associated with mentioned angular momentum is:

$$E_{rot} = \frac{Iw^2}{2} = \frac{L^2}{2I} \tag{2.6}$$

Where I is the rotational inertia and w is the angular velocity.
The quantization of angular momentum implies that rotational energy is also quantized. According to Schrödinger Equation, rotational energy equals to:

$$E_{rot} = \frac{J(J+1)\hbar^2}{2J} \qquad J = 0, 1, 2, ... \tag{2.7}$$

[2]Debye is a CGS unit of electric dipole moment which in SI, 1 D equals $\sim$ 3.33564 coulomb-meter.

Where J is the rotational energy levels. The change of energy for the transition between J and $J-1$ is ΔE_{rot} and the related frequency is defined as:

$$\nu = \frac{\Delta E_{rot}}{h} \tag{2.8}$$

Where h is the Planck's Constant.
According to the relation (2.8), the frequency of electronic, vibrational or rotational transition is proportional to the energy difference between the levels and consequently the frequency ν_{2-1}=230.538 GHz of CO rotational transition, is related to the energy difference between $J=1$ and $J=2$ states.

2.3 Einstein Coefficients

Einstein coefficients describe the probabilities of absorption (excitation) or emission (de-excitation) of photons by an atom or a molecule. An emission line appears when an atom or a molecule makes a transition from higher energy level E_2 to the lower E_1 level. In this case, a photon with a specific frequency and energy equal to the energy difference between two levels, is emitted. An absorption line appears when an atom or molecule makes a transition from lower energy level E_1 to the higher E_2 level. In this case, a photon with a particular frequency and energy equal to the energy difference between two levels, is absorbed. There are 5 different processes for excitation or de-excitation between energy states.

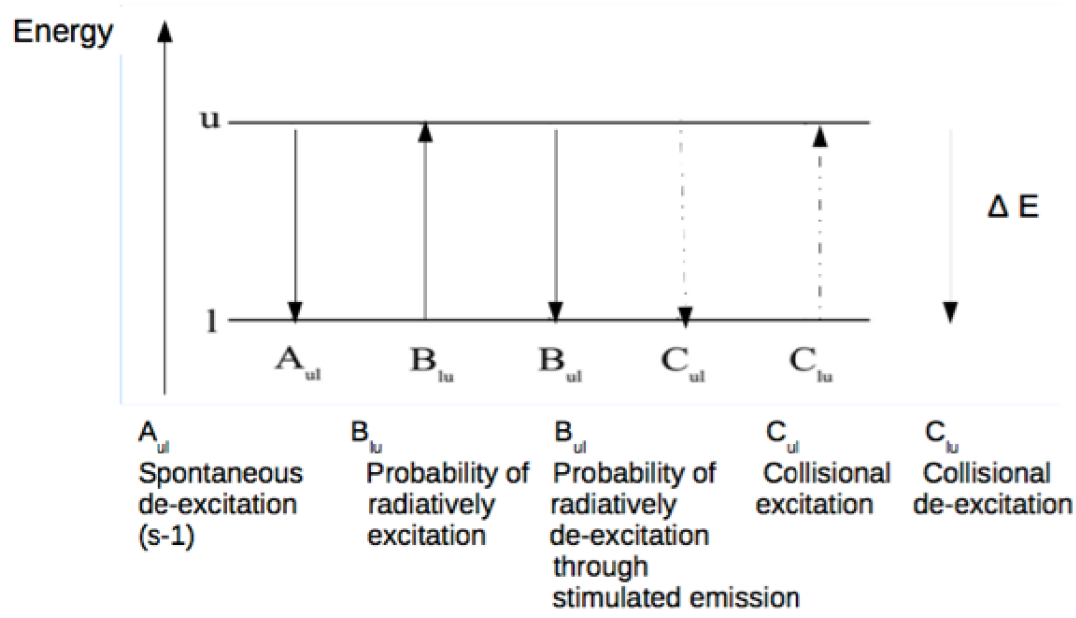

Figure 2.4: 5 different process for excitation and de-excitaion between energy levels in atoms or molecules

Figure 2.4 shows these different processes in which "u" refers to the upper-state and "l" refers to the lower-state. Spontaneous de-excitation, as it is clear from its names, happens when an atom or a molecule go to the ground state spontaneously and

emits a photon. Second processes are called radiatively excitation or de-excitation and it happens when an atom or a molecule absorbs energy from photons and goes to the higher or lower states. The last processes are called collisional excitation or de-excitation. It happens when the density of atoms or molecules is high, so that they can make transitions between levels through colliding each other.
Einstein A and B coefficient are defined as:

$$A_{ul} = \frac{64\pi^4}{3hc^3}\nu^3 \mid \mu_{ul} \mid^2 \tag{2.9}$$

and

$$B_{ul} = \frac{g_l}{g_u}B_{lu} \tag{2.10}$$

Where μ_{ul} is the molecular dipole moment and g_l and g_u are the statistical weights of upper and lower states. The relation between Einstein's coefficients is:

$$A_{ul} = \frac{2h\nu^3}{c^2}B_{ul} \tag{2.11}$$

Considering the spontaneous transitions, $t_A = 1/A_{ul}$ is defined as the time of spontaneous de-excitation of particles. t_{Coll} is the time of collisional de-excitation of particles and defined as:

$$t_{Coll} = \frac{1}{n\sigma < v >} \tag{2.12}$$

Where n is the density of atoms or molecules, σ is the collisional cross section and $< v >$ is the mean velocity of the particles.
In order to get the collisional de-excitation to be the dominant process, it is needed to $t_{Coll} < t_A$:

$$\frac{1}{n\sigma < v >} < \frac{1}{A_{ul}} \tag{2.13}$$

Likewise:

$$n > \frac{A_{ul}}{\sigma < v >} = n_{crit} \tag{2.14}$$

If the density of the target species, is larger than critical density, then the transition process is dominated by collisions (Wilson et al.,2013). In this case, it can be stated that the excitation (or de-excitation) temperature can be counted as kinetic temperature of the particles which implies that, particles are in Local Thermodynamic Equilibrium (LTE).

2.4 Radiative Transfer

The intensity of radiation will remain unchanged along the path of ray if, it is transferred in vacuum. It only changes while passing through a medium whereby intensity of radiation can be removed (absorption coefficient κ) or added (emission coefficient ϵ). The change of intensity of radiation is described by the radiative transfer equation:

$$\frac{dI_\nu}{ds} = -\kappa_\nu I_\nu + \epsilon_\nu \tag{2.15}$$

Where s is the propagation path along the line of sight and I is the intensity of radiation. Absorption κ and emission coefficients ϵ are defined in terms of Einstein coefficients as following:

$$\kappa_\nu = \frac{h\nu}{4\pi}(n_l B_{lu} - n_u B_{ul})\phi_\nu \tag{2.16}$$

and

$$\epsilon_\nu = \frac{h\nu}{4\pi} A_{ul} n_u \tag{2.17}$$

ϕ_ν is the line profile function which describes the distribution of emission or absorption around the transition frequency and it is normalized to unity when integrated over the line:

$$\int_{\Delta\nu} \phi_\nu d\nu = 1 \tag{2.18}$$

Since the propagation path is unknown for measured radiation, it is convenient to define a variable called optical depth τ_ν as:

$$d\tau_\nu = \kappa_\nu ds, \tag{2.19}$$

Where it has been used in the way the radiation propagates in the direction of increasing optical depth.
Rewriting equation (2.15) in terms of optical depth, leads to get the following relation:

$$\frac{dI_\nu}{d\tau_\nu} = S_\nu - I_\nu \tag{2.20}$$

Where the source function S_ν is defined as:

$$S_\nu = \frac{\epsilon_\nu}{\kappa_\nu} \tag{2.21}$$

By multiplying both sides of the equation (2.20) by the factor of e^{τ_ν} and then, integration from optical path 0 to τ_ν, a very general solution is achieved:

$$I_\nu = I_\nu(0)e^{-\tau_\nu} + S_\nu(1 - e^{-\tau_\nu}) \tag{2.22}$$

If the radiation comes from a black body source (a hypothetical ideal body which emits or absorbs energy as a spectrum at all electromagnetic frequencies which is defined only by its temperature) and that body is in thermal equilibrium, the source function (spectral radiance) will be equal to the Planck function ($S_\nu = B_\nu$) which is given by:

$$B_\nu(\nu, T) = \frac{2h\nu^3}{c^2} \frac{1}{exp(\frac{h\nu}{kT}) - 1} \tag{2.23}$$

Where c is the speed of light and k is the Boltzmann's constant.

If the radiation occurs in a very optically thick medium in which, the mean free path of the particles is smaller than the scale of the temperature variation, the system is experiencing Thermodynamic Equilibrium (TE) or Local Thermodynamic Equilibrium (LTE). It means that in this case, the temperature of black-body radiation can be assumed as the excitation temperature ($B_\nu(T) = B_\nu(T_{ex})$).
Using Rayleigh-Jeans approximation ($h\nu << kT$) for long wavelengths (low frequencies), the relation between intensity and observed brightness temperature is derived as:

$$T_b = \frac{c^2}{2k\nu^2} B_\nu(T) = \frac{\lambda^2}{2k} B_\nu(T) \tag{2.24}$$

And the relation between intensity and total flux is given by (Wilson et al.,2013):

$$S_\nu = B_\nu(T)\Delta\Omega \tag{2.25}$$

In which S_ν is expressed in Jansky (Jy). Jansky is a non-SI unit for flux density and it is equivalent to 10^{-26} W m^{-2} Hz^{-1}. $\Delta\Omega$ is the solid angle of Callisto viewed from Earth and is defined as:

$$\Delta\Omega = \frac{area}{distance^2} = \frac{\pi R_{Callisto}^2}{d^2} \tag{2.26}$$

Where d is the distance between Earth and Callisto, which is different for different observations.
Rewriting radiative transfer equation in terms of T_b, an equivalent solution will be derived as:

$$T_b = T_{bg} e^{-\tau_\nu} + T_{ex}(1 - e^{-\tau_\nu}) \tag{2.27}$$

Where T_b is the observed brightness temperature, T_{bg} is the background temperature (the temperature of the environment in which the target is located) and T_{ex} is the temperature of excitation. Considering two relations (2.22) and (2.27), if the target medium is optically thick ($\tau_\nu >> 1$), the measured intensity will be the black body radiation distribution at the excitation temperature, and the observed brightness temperature will be equal to the excitation temperature.
Observing emission or absorption lines, depends on the value of $T_{ex} - T_{bg}$. If it is larger than zero (positive), then the excitation temperature will be larger than the background temperature ($T_{ex} > T_{bg}$) and emission lines will be detected.
In the case of observing absorption lines, the excitation temperature will be smaller than the background temperature ($T_{ex} < T_{bg}$) and relation (2.27) will be summarized as:

$$T_b = T_{bg} e^{-\tau} \tag{2.28}$$

According to this relation, the optical depth can be easily derived from the spectrum of absorption lines as:

$$\tau = ln(\frac{T_{bg}}{T_b}) \tag{2.29}$$

Where T_{bg} is the temperature of the continuum and T_b is the derived brightness temperature of the detected line. The extracted spectrum will not show any absorption or emission lines if, $T_{bg} = 0$ or $T_{ex} = 0$ respectively.

2.5 Column Density

Calculation of molecular column density from molecular spectral lines is a very strong tool to derive the properties of the medium from which, the molecular lines are extracted. Column density is a quantity that describes the number of particles per unit area along the line of sight. it can be defined as the number of particles in energy level u, integrated over the path length ds:

$$N_u = \int n_u ds \tag{2.30}$$

For a system in thermal equilibrium, the relative population of different levels is defined by Boltzmann distribution:

$$\frac{n_u}{n_l} = \frac{g_u}{g_l} e^{-h\nu_{ul}/kT_{ex}} \tag{2.31}$$

Where n_u and n_l are the population of upper and lower states and g_u and g_l are the statistical weights (degeneracy) of the upper and lower states, respectively.
Now by using the definitions of optical depth (2.19), absorption coefficient κ_ν (2.16), the Boltzmann equation (2.31), the definition of the column density (2.30) to relate optical depth to the number of particles in the upper level N_u, using the relation $d\nu/\nu = dv/c$ to turn the frequency to the velocity and the value of A_{ul} ($A_{21}(CO) = 7.1 \times 10^{-7} s^{-1}$) (Wilson et al.,2013), a relation for N_u will be extracted:

$$N_u = \frac{8\pi\nu^3}{c^3}[exp(\frac{h\nu}{kT}) - 1]^{-1} \times {A_{ul}}^{-1} \int \tau_\nu dv \tag{2.32}$$

The value of N_u demonstrates the total population of the particles in the upper state. In order to relate this value to the total population (N_{tot}) of particles in all energy levels (total column density), the relation of Boltzmann distribution can be used. By exchanging n_l with N_{tot} and assuming that the excitation temperature is constant and is the same for all transitions, relation (2.31) is rephrased as:

$$\frac{N_u}{N_{tot}} = \frac{g_u}{Q_{rot}} e^{-E_u/kT_{ex}} \tag{2.33}$$

Where Q_{rot} is the rotational partition function which characterizes the comparative population of levels. It equals the sum of all statistical weights and depends on the temperature:

$$Q_{rot} = \Sigma g_i e^{-E_i/kT} \tag{2.34}$$

Substituting N_u from equation (2.32) in equation (2.33) and using equation (2.34), a relation to calculate total column density will be derived as:

$$N_{tot} = \frac{8\pi\nu^3}{c^3} \frac{Q_{rot}}{g_u} exp(\frac{E_u}{kT_{ex}}) \times [exp(\frac{h\nu}{kT}) - 1]^{-1} \times {A_{ul}}^{-1} \int \tau_\nu dv$$

(2.35)

g_u for CO is given by:

$$g_u = (2J_u + 1) \tag{2.36}$$

For a linear molecule such as CO, Q_{rot} will be approximated to (Mangum and Shirley,2015):

$$Q_{rot} \approx \frac{kT_{ex}}{hB} \tag{2.37}$$

Where B is the rigid rotor rotational constant measured in Hz.
Since in this thesis, no strong line is detected in extracted spectra of CO, it can be assumed that CO is optically thin in the atmosphere of Callisto. On the other hand, Rayleigh-Jeans approximation ($h\nu << kT_{ex}$) is valid for CO $J = 2 - 1$ transition frequency and Callisto's temperature (120 K). Using these assumptions, the relation of total column density will be simplified to:

$$N_{tot}^{thin} = \frac{8\pi\nu^2}{c^3}\frac{k^2{T_{ex}}^2}{h^2 B g_u} \times exp(\frac{E_u}{kT_{ex}}) \times {A_{ul}}^{-1} \int T_b dv \tag{2.38}$$

For a Gaussian line, $\int T_b dv$ is the integrated brightness temperature. It equals to the line peak intensity in terms of temperature (in K) times the line full width half maximum in terms of velocity (in km/s).
For a target object which is optically thick ($\tau >> 1$), the total column density is defined as:

$$N_{tot} = N_{tot}^{thin}\frac{\tau}{1 - exp(-\tau)} \tag{2.39}$$

3

Method

3.1 ALMA archive query

ALMA archive[1] is used to pick up all available interferometric data of Callisto at the frequency of CO $J = 2 - 1$ transition (230.538 GHz).
Considering this fact that the higher energy states have higher temperature and comparing with the temperature of Callisto, transitions in the lower sates are most likely to happen. Therefore, searching for transitions between three lower states began. But since there were not useful projects in ALMA archive for ($J = 1 - 0$ or $J = 3 - 2$), $J = 2 - 1$ transition is chosen to search for related data of CO in Callisto from ALMA online archive.
Figure 3.1 shows the page of ALMA archive in which by selecting and writing some properties of target projects, the related data will be accessible.

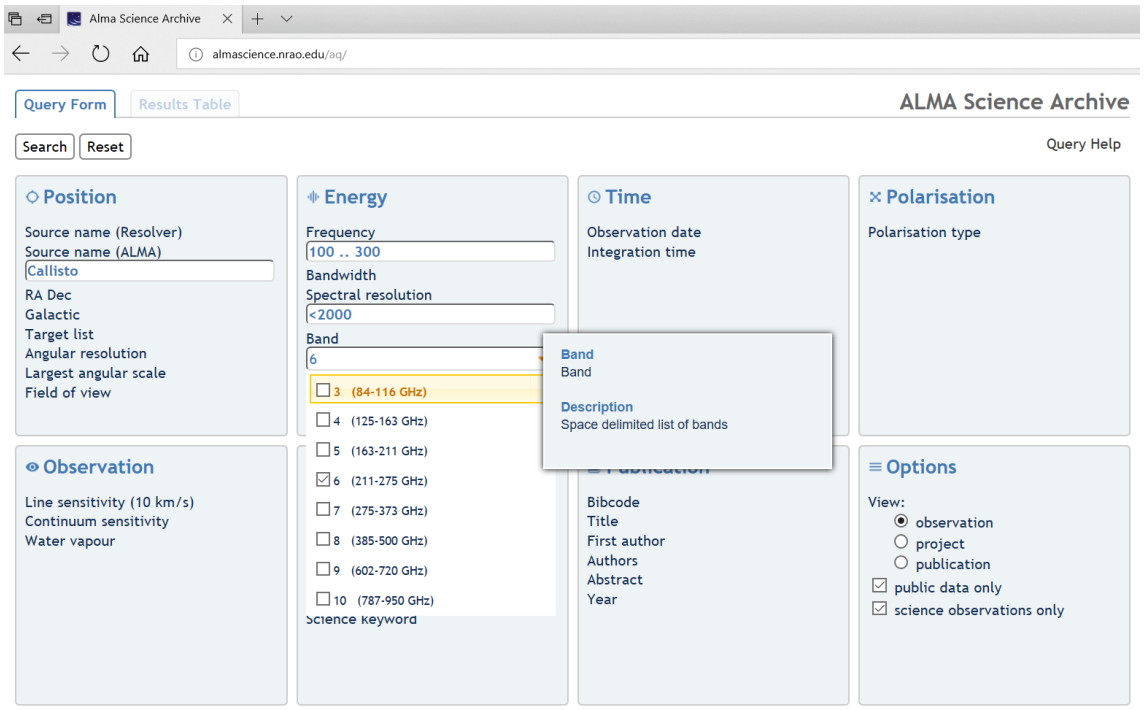

Figure 3.1: ALMA archive query

[1]https://almascience.nrao.edu/alma-data/archive

After defining Callisto as the ALMA source name and the interval of frequency in which the target frequency exists, determining the spectral resolution is required. Spectral resolution of a spectrum describes its ability to resolve the appeared spectral lines and it is usually denoted by $\Delta\nu$ (FWHM) in Hz. Resolving power of an instrument is defined as:

$$P = \frac{\nu}{\Delta\nu} \tag{3.1}$$

$P < 1000$ is regarded as low spectral resolution which leads to losing much information from spectrum and spectral lines will not be resolved. $1000 < P < 10000$ is considered as intermediate resolution which is used for broadest spectral lines. $10000 < P$ is regarded as high spectral resolution which is used to study narrow spectral lines.
The results of the density profile of introduced atmosphere model, shows that H_2O and CO have almost the same profile and they follow the same trajectory in the atmosphere of Callisto. Referring the detection of water lines from Callisto's atmosphere and the results of atmosphere model, it can be assumed that CO and H_2O are mixed well with each other and they move with approximately the same velocity in the atmosphere of Callisto. Therefore, it is expected that CO lines would have approximately the same width of detected water lines ($\Delta v \sim$1.35 km/s). Thus, choosing a spectral resolution better than 1 MHz (1.3 km/s), will give spectra with high resolution to be able to detect CO lines.
In the band section, the band 6 in which the target frequency is included is chosen. Afterwards all required parameters are selected, the related projects can be downloaded via ALMA archive URL. Then, the data reduction is executed with CASA, which is an astronomy software used to process both interferometric and single dish data. This software has different versions so that each project and even different files of a project may be worked with a different CASA version.

3.2 Extract the data and spectra

When the related projects have been downloaded and the data which are in the form of zip files are extracted, the right version of CASA for each project must be determined. The file with README suffix reveals the right version of CASA, especially for mentioned files and clarifies if CASA needs to be run as "Manually" or "pipe-line". Then, the step called data reduction can be run, successfully.
It is noteworthy that not all reduced data will be useful. The data that have been collected with the compact array or in single dish mode, are not used in this project, because they are neither sensitive enough nor belong to the interferometric measurements.
Afterwards all reduced data are created and the fitting is performed, taking out the

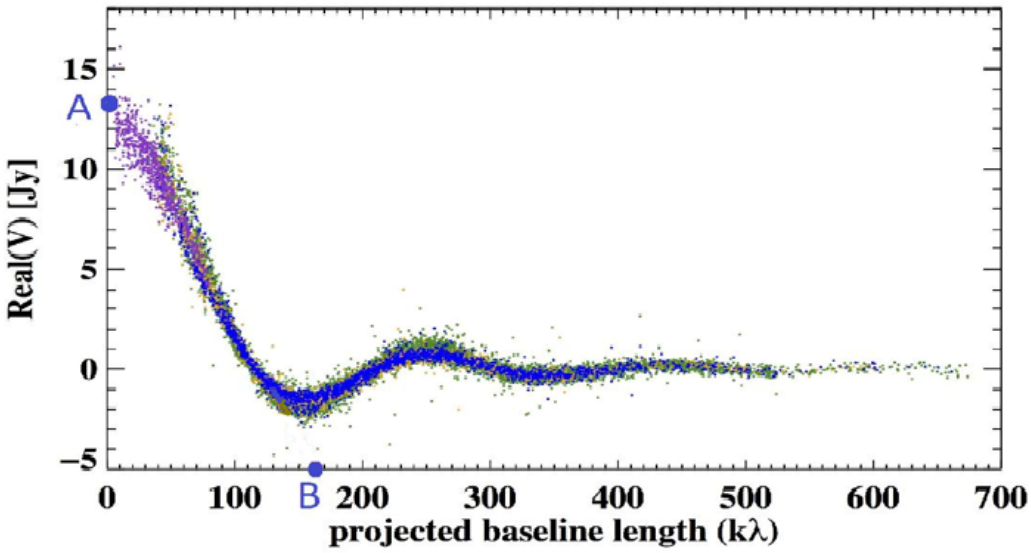

Figure 3.2: The colored points are the measured visibilities by the array of an interferometer. Point A is fitted to define the total flux (amplitude of the visibility) which can not be measured by interferometry and point B is fitted to find the diameter of the target source.

data related to Callisto and the spectra in TOPO[2] mode, regridding the spectra, flagging, realign the spectra in Callisto's frame and averaging all spectra to gain final one, are the next steps respectively.
Extracting the data and spectra are done with a fitting program called UVFit (Written by:S.Muller-Ivan M.Vidal) which extracts total flux of the visibilities, while running in casapy-4.7.
Since the data are observed and collected at different times and different distances from Callisto, consequently the diameter of Callisto is different for all of them. Thus, first of all the spectra must be fitted to the diameter of Callisto, then averaging the spectra is possible and reliable.
To be able to fit the measured visibilities, there must be a reference model to be compared. In this model, Callisto has been considered as a circular disc on the sky. Then, the Fourier transform of the intensity distribution of the defined model is computed at the U and V coordinates of the used baselines. The computed Fourier transform will give a model for visibilities. Comparing the observed visibilities with computed visibilities based on the assumed model, leads to find the best fitted result of visibilities.
In the figure 3.2, the colored points are the measured visibilities by the array of an interferometer which is fitted to point A and B. As it is clear in the image, amplitude of the visibility decreases and gets lower as the baseline increases. If the visibilities of a source goes to zero on the longest baseline, it will be resolved which leads to find the diameter of the source (point B).

[2] TOPO is the topocentric frequency reference frame in CASA in which Earth has been assumed to be fixed in its position and the target body (Callisto) is moving with respect to the Earth.

Regridding, is the process of interpolating from one grid resolution to a different grid resolution. All observations have their own three parameters: The number of channels, frequency and Δfrequency (resolution). After regridding, these parameters must be the same for all observations. Note that, it is not possible to increase the resolution, it can just be decreased.
Extracted spectra may contain some Earth atmospheric lines like CO or O_3 which must be flagged (removed) from spectra, to avoid contamination in the final averaged spectra. Deriving the relative velocity of Callisto with respect to the Earth from Jet Propulsion Laboratory(JPL ephemeris)[3], makes it possible to calculate the doppler shift of the detected lines and realign the spectra in Callisto's rest frame, instead of TOPO mode. Thereafter, averaging the spectra will be performed in Matlab.

3.3 Correcting Doppler Effect

The Doppler effect is a phenomena in which the frequency or wavelength of a radiation is changed for an observer who is moving with respect to the source of radiation. A general equation for Doppler effect is given by:

$$\Delta f = \frac{\Delta v}{c} f_0 \tag{3.2}$$

Where Δf is the difference between observed and emitted frequency, f_0 is the emitted frequency, Δv is the velocity of the receiver (Earth) relative to the source (Callisto) and c is the speed of light. Δv is positive when the source is moving towards the Earth and negative, when it is receding.
In the case of observing from the surface of the Earth, there are four types of revolution: Rotation of Earth around the Sun, rotation of Callisto around Jupiter, rotation of Jupiter around the Sun and Earth rotation. The result of these movements is that, depending on the position of Jupiter with respect to the Earth, sometimes Callisto moves toward the Earth and some times it recedes. As a consequence, the measured data will not be the same for different observations and the target lines will be shifted positively or negatively with respect to the rest frequency. Doppler correction in this thesis is done by a dedicated task called "cvel" which transforms the visibilities to an appropriate reference frame.

[3]https://ssd.jpl.nasa.gov/horizons.cgi

3.4 Available ALMA data

Table 3.1 presents all available projects in ALMA online archive, which contain raw data related to Callisto, associated with the target frequency (230.538 GHz) and are collected by interferometry. It also shows the version of CASA used for each project and the names of the reduced data files after running in CASA.
JPL ephemeris indicates the relative motion of the source (Callisto) with respect to the observer (Earth). Whereas in the mentioned doppler effect in previous part, it has been assumed that the observer moves with respect to the source. Therefore, the sign of the relative motion in JPL is unlike the sign of mentioned relative velocity of doppler effect. In JPL, if the relative velocity is negative it means the target body moves toward the observer (observing leading hemisphere of Callisto) and if it is positive, it mean the source moves away (observing trailing hemisphere of Callisto).

Alma project ID	CASA version	Callisto reduced data	Observing date	Hemisphere
2012.1.00013.s	4.2.1	X11f4.ms.split.cal	14-Dec-2013	Leading
2012.1.00013.s	4.2.1	X842.ms.split.cal	11-Jan-2014	Trailing
2012.1.00013.s	4.2.1	X3c7.ms.split.cal	15-Jan-2014	Leading
2012.1.00013.s	4.2.1	X6f8.ms.split.cal	15-Jan-2014	Leading
2012.1.00013.s	4.2.1	X52.ms.split.cal	28-Apr-2014	Trailing
2012.1.00013.s	4.2.1	X1db5.ms.split.cal	11-Dec-2014	Leading
2012.1.00013.s	4.2.1	X183d.ms.split.cal	11-Dec-2014	Leading
2012.1.00640.s	4.2.1	X376.ms.split.cal	03-Apr-2014	Trailing
2012.1.00377.s	4.2 pipeline	X1e9b.ms.split.cal	28-Dec-2014	Leading
2012.1.00377.s	4.2 pipeline	X25b1.ms.split.cal	25-Dec-2014	Leading
2012.1.00377.s	4.2 pipeline	X65b.ms.split.cal	29-Jan-2014	Trailing
2012.1.01069.s	4.2.0	X15b4.ms.split.cal	04-Nov-2013	Leading
2013.1.00210.s	4.3.1	X25de.ms.split.cal	11-Dec-2014	Leading
2013.1.00210.s	4.3.1	X5c3.ms.split.cal	10-Dec-2014	Leading
2013.1.00661.s	4.2 pipeline	X99e.ms.split.cal	29-Jan-2015	Trailing
2013.1.00773.s	4.2 pipeline	Xba2.ms.split.cal	04-Apr-2015	Trailing
2013.1.00862.s	4.3	X2186.ms.split.cal	11-Dec-2014	Leading
2013.1.00319.s	4.2 pipeline	X340.ms.split.cal	29-Jan-2015	Trailing
2013.1.00457.s	4.2 pipeline	X1b87.ms.split.cal	28-Dec-2014	Leading

Table 3.1: Extracted ALMA projects and reduced data associated with Callisto. Each project must be worked with the right particular version of CASA. These observations have been done at different periods of time, while detecting different hemispheres of Callisto.

4

Results

4.1 Characteristics of datasets

Table 4.1 illustrates the extracted information related to Callisto from all the projects. The first column of the table shows the name of the projects as well as the time of the observations. The second column is the observed frequency in GHz and the third one is the angular diameter of Callisto in arc-second, derived via UVFit program.
By using tools of the Sub-millimeter Array Observer Center (SMA-ObserverCenter)[1], the angular size and visibility flux of Callisto for given date and frequency can be generated. These quantities are predictions of a model under simplifying assumptions which are shown in columns 4 and 6 of table 4.1, for comparison.
Measured total flux (fifth column of the table 4.1) and size of Callisto from ALMA observations (third column of the table 4.1) are not compatible with the predictions of the defined simple model. The appeared discrepancy may arise due to the imperfection in the assumed models.
Seventh column of the table 4.1 shows the relative velocity of Callisto with respect to the Earth[2] and the last column illustrates the distance of Callisto from the Earth, achieved from JPL ephemeris and expressed in Astronomical Unit[3] (AU=1.496×10^8 km). It may also be calculated by using the extracted angular diameter of Callisto (table 4.1). If the distance between two objects (D) is much larger than the diameter of target body (d), the relation between distance and angular size (δ) is given by:

$$\delta \simeq 180/\pi \times 3600 \times d/D \tag{4.1}$$

In which $180/\pi \times 3600$ converts radian to arcsecond. The diameter of Callisto is 4821 km (Anderson et al.,2001) and the angular size of Callisto can be read from the table. Obviously, if the angular size is bigger the distance must be smaller which is shown in the table 4.1.
The derived angular size of Callisto based on the assumed model from SMA observer center, is constant for each project. Callisto has been assumed as a back-body in SMA models and hence, its brightness temperature is 120 K and it is constant for all projects.
As it can be seen clearly in the table 4.1, the received flux in Jy is inversely proportional to square of the distance and less flux is received in longer distances.

[1] http://sma1.sma.hawaii.edu/planetvis.html
[2] https://ssd.jpl.nasa.gov/horizons.cgi
[3] Astronomical Unit is a unit for length and equals the distance from Earth to the Sun.

Project ID	Frequency (GHz)	UV-fit size (″)	Predicted size (″)	UV-fit Flux (Jy)	Predicted Flux (Jy)	Rel. Velocity (km/s)	Distance (AU)
2012.1.00377.s	214.3817	1.5065±0.0008	1.5400	6.5965±0.0020	7.104	+11.7	4.31
29-Jan-2014	216.0700	1.4981±0.0006	„	6.6849±0.0019	7.214	„	„
	227.5580	1.4960±0.0006	„	7.5450±0.0021	7.983	„	„
	229.2463	1.4974±0.0008	„	7.6699±0.0028	8.099	„	„
2012.1.00640.s	217.4400	1.2458±0.0002	1.2870	4.6734±0.0008	5.101	+32.4	5.18
03-Apr-2014	219.8984	1.2455±0.0002	„	4.7793±0.0009	5.215	„	„
	230.0302	1.2445±0.0003	„	5.2953±0.0014	5.695	„	„
	230.9907	1.2433±0.0002	„	5.3626±0.0011	5.741	„	„
2012.1.00013.s	219.6113	1.1651±0.0004	1.1990	4.1826±0.0017	4.515	+20.5	5.55
28-Apr-2014	220.4297	1.1646±0.0008	„	4.2806±0.0031	4.548	„	„
	230.4503	1.1644±0.0004	„	4.6407±0.0019	4.960	„	„
	230.6984	1.1624±0.0002	„	4.6516±0.0011	4.971	„	„
2013.1.00862.s	213.2963	1.3517±0.0005	1.3810	5.2931±0.0014	5.657	-30.2	5.26
11-Dec-2014	228.6186	1.3495±0.0001	„	6.1445±0.0005	6.478	„	„
	230.4570	1.3500±0.0002	„	6.2160±0.0010	6.580	„	„
	230.5722	1.3506±0.0003	„	6.2233±0.0011	6.567	„	„
2012.1.00377.s	214.3560	1.4077±0.0003	1.4390	5.7715±0.0007	6.202	-21.8	5.04
25-Dec-2014	216.0441	1.4098±0.0001	„	5.8631±0.0004	6.297	„	„
	227.5307	1.4073±0.0001	„	6.6175±0.0005	6.968	„	„
	229.2188	1.4074±0.0001	„	6.7168±0.0005	7.070	„	„
2012.1.00377.s	214.3569	1.4074±0.0001	1.4460	5.7971±0.0005	6.262	-30.3	5.00
28-Dec-2014	216.0450	1.4071±0.0001	„	5.8902±0.0005	6.359	„	„
	227.5317	1.4047±0.0001	„	6.6458±0.0006	7.036	„	„
	229.2198	1.4048±0.0001	„	6.7463±0.0006	7.139	„	„
2013.1.00457.s	218.3081	1.4199±0.0007	1.4460	6.0939±0.0023	6.490	-30.1	5.00
28-Dec-2014	220.4010	1.4197±0.0002	„	6.1904±0.0008	6.612	„	„
	230.5109	1.4180±0.0002	„	6.8323±0.0009	7.217	„	„
	232.7869	1.4190±0.0007	„	6.9488±0.0028	7.357	„	„
2013.1.00319.s	213.0121	1.4933±0.0005	1.5240	6.4269±0.0019	6.671	+3.6	4.35
29-Jan-2015	215.0101	1.4925±0.0005	„	6.5479±0.0019	6.997	„	„
	227.5654	1.4918±0.0006	„	7.3575±0.0024	7.618	„	„
	229.8485	1.4928±0.0002	„	7.5352±0.0010	7.972	„	„
2013.1.00661.s	217.5690	1.4889±0.0002	1.5240	6.6392±0.0007	7.161	+3.5	4.36
29-Jan-2015	219.4442	1.4840±0.0003	„	7.7487±0.0011	7.262	„	„
	229.6650	1.4866±0.0002	„	7.5253±0.0009	7.960	„	„
	231.6200	1.4868±0.0003	„	7.6527±0.0012	8.092	„	„
2013.1.00773.s	215.2406	1.3581±0.0007	1.3860	5.4199±0.0021	5.600	+32.1	4.79
04-Apr-2015	217.2408	1.3562±0.0011	„	5.5204±0.0034	5.906	„	„
	229.1179	1.3576±0.0002	„	6.2019±0.0008	6.553	„	„
	232.3048	1.3565±0.0008	„	6.3253±0.0030	6.732	„	„

Table 4.1: The extracted flux and fitted diameter related to each project are presented. Angular size and flux based on a simplified model are obtained by using tools of SMA observer center. Relative velocity and distance of Callisto from the Earth are obtained via JPL ephemeris. The sign of relative motion reveals the associated hemisphere of Callisto. The observation times of the projects are shown again to be identified faster .

4.2 Characteristics of extracted spectra

All the spectra associated with the presented extracted data in table 4.1 are plotted in Appendix A. These spectra are in TOPO mode in which the Earth is assumed as a reference which is stationary and Callisto is moving with respect to the Earth. In this case, the line at the position of $CO_{J=2-1}$ transition frequency (230.538 GHz), belongs to the CO of Earth's atmosphere. The position of CO line in the atmosphere of Callisto can be calculated via line shift by using Callisto's relative velocity, which is shown in table 4.1.
The measurements of the projects have been done in 4 different frequency bands. The lowest frequency of each band is given in the second column of the table 4.1. After gridding the spectra, the final and remained frequency bands are plotted in different colors in figures A.1-A.10. In each figure, two (or three) dotted lines are plotted at the positions of $CO_{J=2-1}$ transition (230.538 GHz) and O_3 (231.28151 GHz and 229.57495 GHz) of Earth's atmosphere.
According to the chosen channel to grid the spectra, some frequency bands may be removed. On the other hand, the beginning and the end of the chosen frequency channel, may not exist in the extracted data. In that case, the total flux value associated to not existing frequency, is defined as zero and it is appeared as the straight lines going down to the zero in the spectra.
The plotted spectra in Appendix A are very broad compared to the detected lines and it is difficult to discern the characteristics of the lines. Thus, they are zoomed and shown with higher resolution, in the following section.

4.3 Spectra in the interval of target frequency

Figures 4.1-4.10 present cut-outs of the reduced spectra covering the frequencies of interest. To be able to see the detected lines, all spectra are shown in zoomed form. Since all spectra are plotted in TOPO mode, the line at the position of $CO_{J=2-1}$ frequency which is marked by a red line, belongs to the Earth's atmosphere and the corresponding frequency doppler shifted to the rest frame of Callisto's atmosphere, is marked by a green line. By using the relation (3.2) for $CO_{J=2-1}$ transition frequency (230.538 GHz) and the relative velocities of Callisto with respect to the Earth (Table 4.1), the values of line shifting (Δf) are calculated. If the sign of the relative velocity is positive, it means Callisto is moving away from the Earth and Δf must be subtracted from CO transition frequency (230.538 GHz) and if it is negative, Δf must be added. In some spectra, atmospheric ozone line is illustrated with a blue line.
Linear fitting, a process to construct the best fit first order polynomial to the data points, and deriving rms noise are done in Matlab straightforwardly. Matlab has a simple tool box to linear fit the spectra. To obtain the rms noise, one needs to use rms command for residuals after linear fitting.

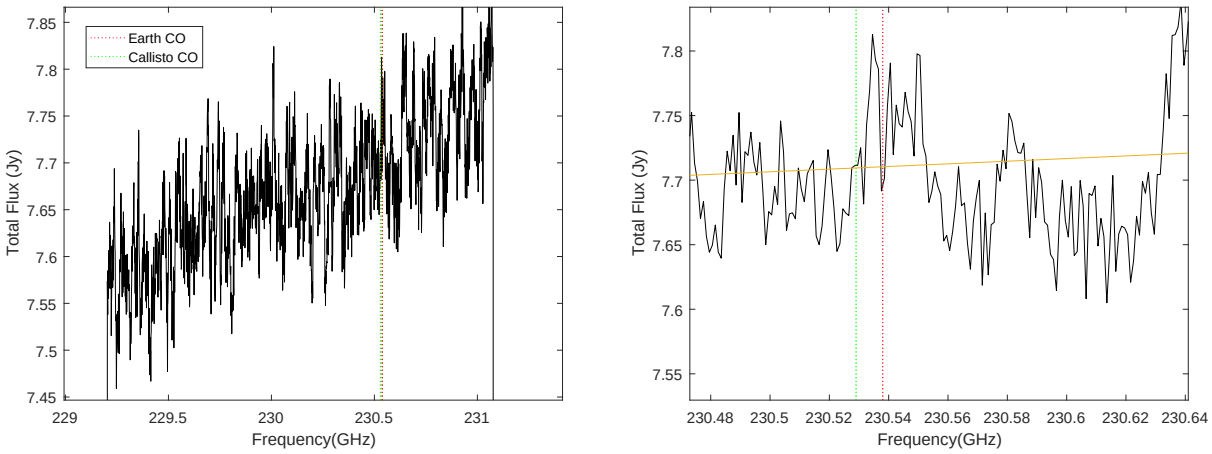

Figure 4.1: The spectrum of the project 2012.1.00377.s in TOPO mode along with a zoom-in of the fitted spectrum with achieved 48.3 mJy rms noise. This project has been observed in 29-Jan-2014. The red dotted line marks the center frequency of CO $(2-1)$ from Earth's atmosphere and the green line marks the doppler-shifted center frequency of the same CO line at Callisto.

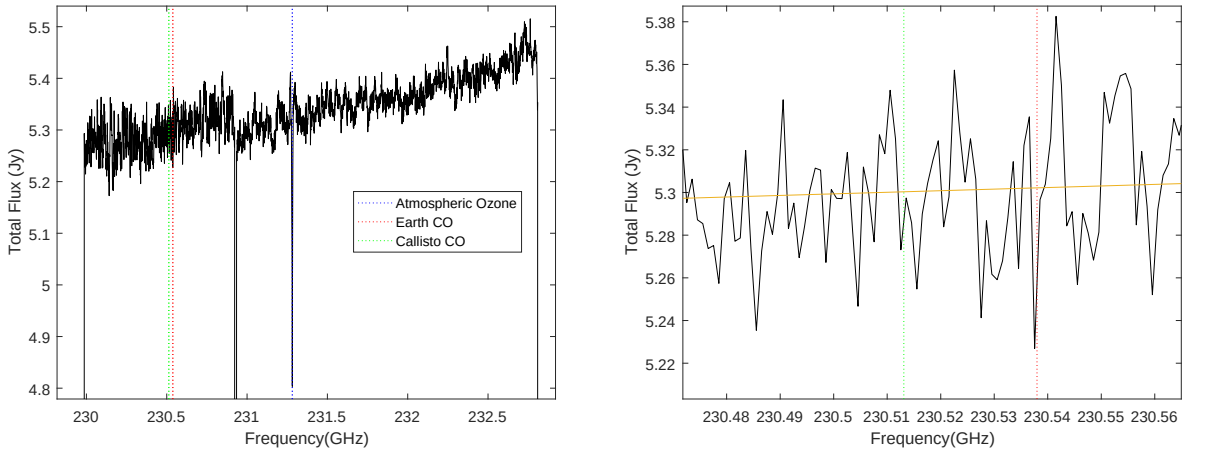

Figure 4.2: The spectrum of the project 2012.1.00640.s in TOPO mode along with a zoom-in of the fitted spectrum with achieved 28.8 mJy rms noise. The red dotted line marks the center frequency of CO $(2-1)$ from Earth's atmosphere and the green line marks the doppler-shifted center frequency of the same CO line at Callisto.

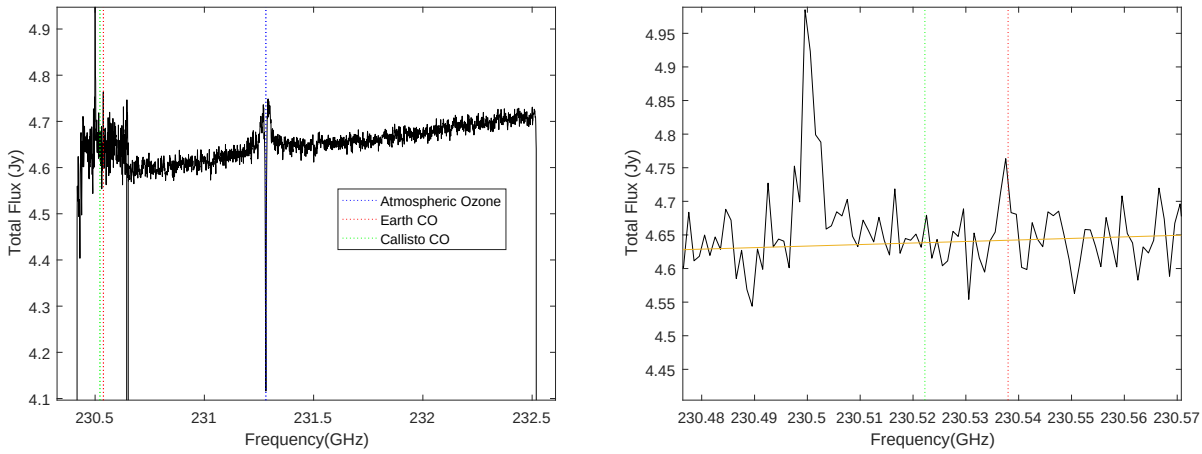

Figure 4.3: The spectrum of the project 2012.1.00013.s in TOPO mode along with a zoom-in of the fitted spectrum with achieved 56.9 mJy rms noise. The red dotted line marks the center frequency of CO $(2-1)$ from Earth's atmosphere and the green line marks the doppler-shifted center frequency of the same CO line at Callisto.

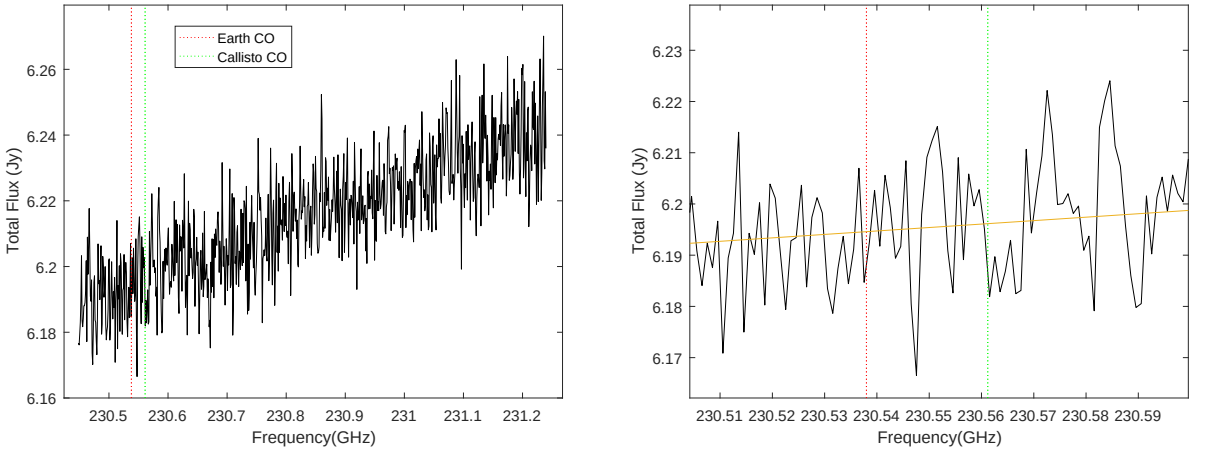

Figure 4.4: The spectrum of the project 2013.1.00862.s in TOPO mode along with a zoom-in of the fitted spectrum with achieved 11.1 mJy rms noise. The red dotted line marks the center frequency of CO $(2-1)$ from Earth's atmosphere and the green line marks the doppler-shifted center frequency of the same CO line at Callisto.

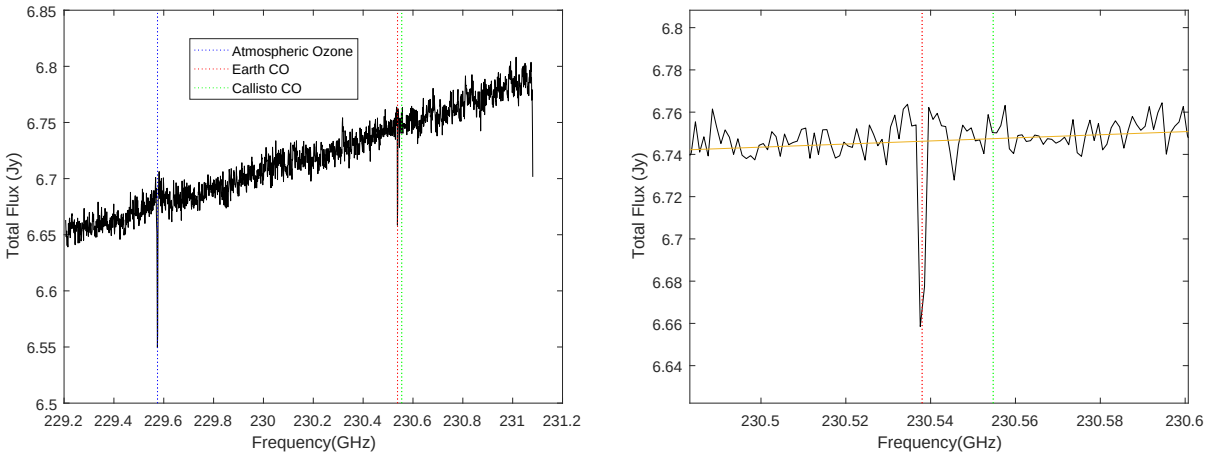

Figure 4.5: The spectrum of the project 2012.1.00377.s in TOPO mode along with a zoom-in of the fitted spectrum with achieved 7.3 mJy rms noise. This project has been observed in 25-Dec-2014. The red dotted line marks the center frequency of CO $(2-1)$ from Earth's atmosphere and the green line marks the doppler-shifted center frequency of the same CO line at Callisto.

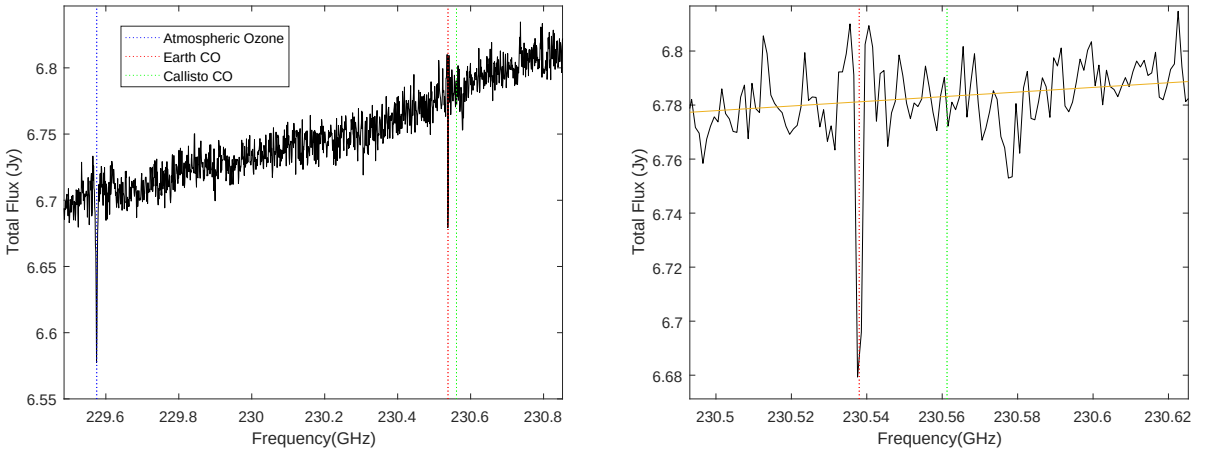

Figure 4.6: The spectrum of the project 2012.1.00377.s in TOPO mode along with a zoom-in of the fitted spectrum with achieved 9.2 mJy rms noise. This project has been observed in 28-Dec-2014. The red dotted line marks the center frequency of CO $(2-1)$ from Earth's atmosphere and the green line marks the doppler-shifted center frequency of the same CO line at Callisto.

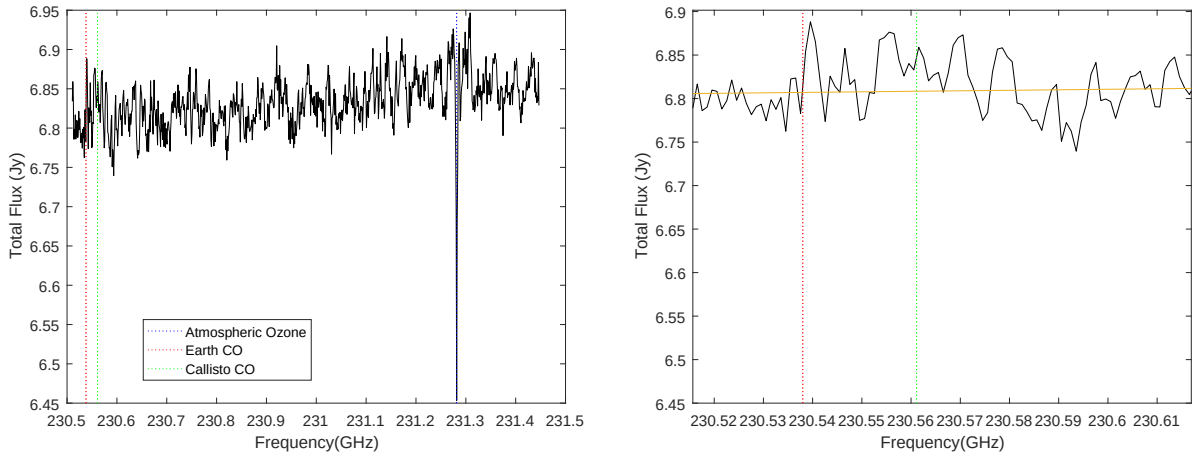

Figure 4.7: The spectrum of the project 2013.1.00457.s in TOPO mode along with a zoom-in of the fitted spectrum with achieved 26.3 mJy rms noise. The red dotted line marks the center frequency of CO $(2-1)$ from Earth's atmosphere and the green line marks the doppler-shifted center frequency of the same CO line at Callisto.

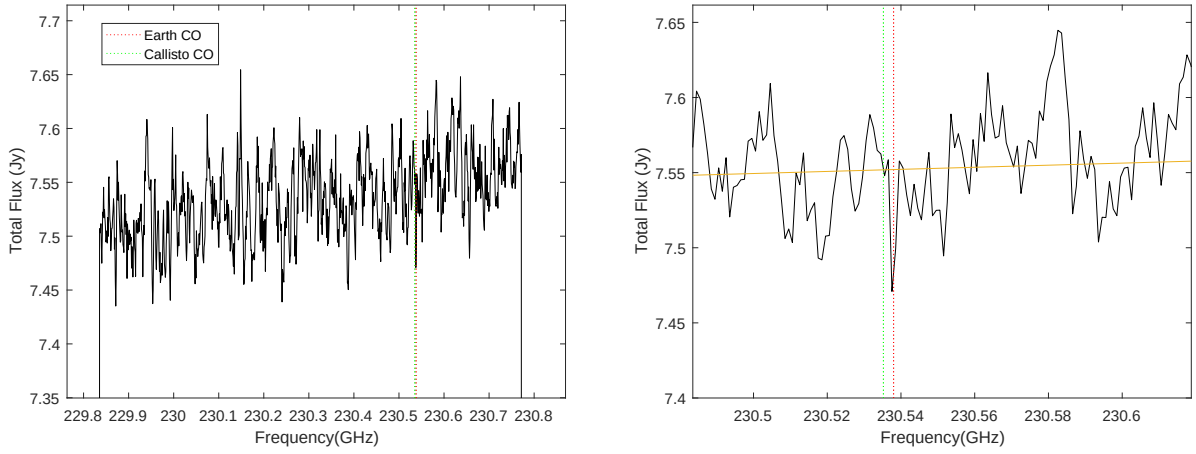

Figure 4.8: The spectrum of the project 2013.1.00319.s in TOPO mode along with a zoom-in of the fitted spectrum with achieved 31.4 mJy rms noise. The red dotted line marks the center frequency of CO $(2-1)$ from Earth's atmosphere and the green line marks the doppler-shifted center frequency of the same CO line at Callisto.

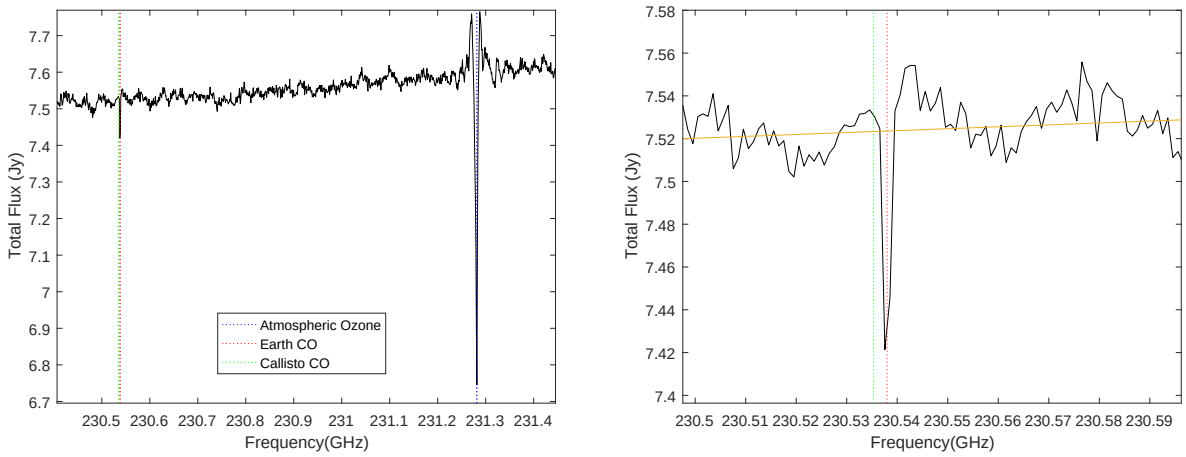

Figure 4.9: The spectrum of the project 2013.1.00661.s in TOPO mode along with a zoom-in of the fitted spectrum with achieved 13.4 mJy rms noise. The red dotted line marks the center frequency of CO $(2-1)$ from Earth's atmosphere and the green line marks the doppler-shifted center frequency of the same CO line at Callisto.

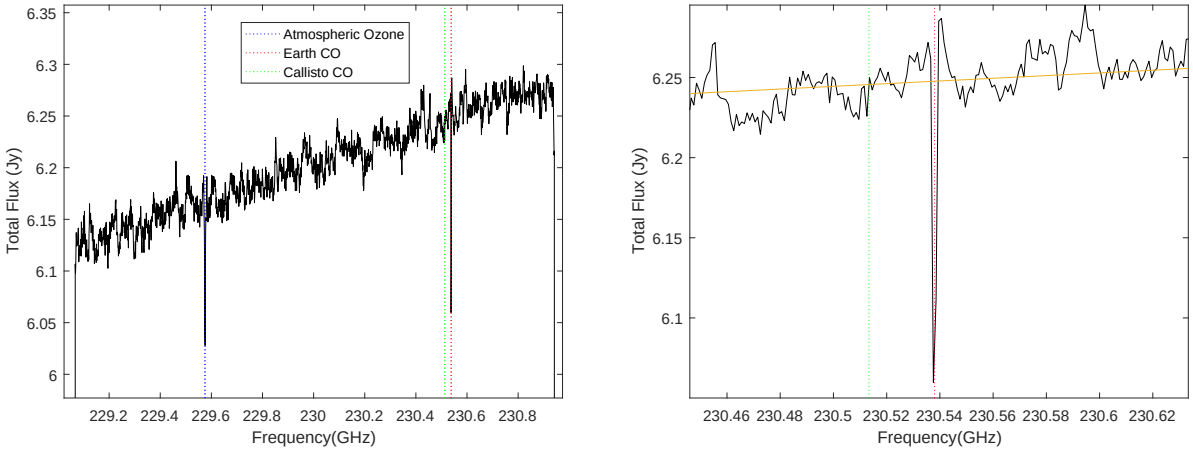

Figure 4.10: The spectrum of the project 2013.1.00773.s in TOPO mode along with a zoom-in of the fitted spectrum with achieved 12.0 mJy rms noise. The red dotted line marks the center frequency of CO $(2-1)$ from Earth's atmosphere and the green line marks the doppler-shifted center frequency of the same CO line at Callisto.

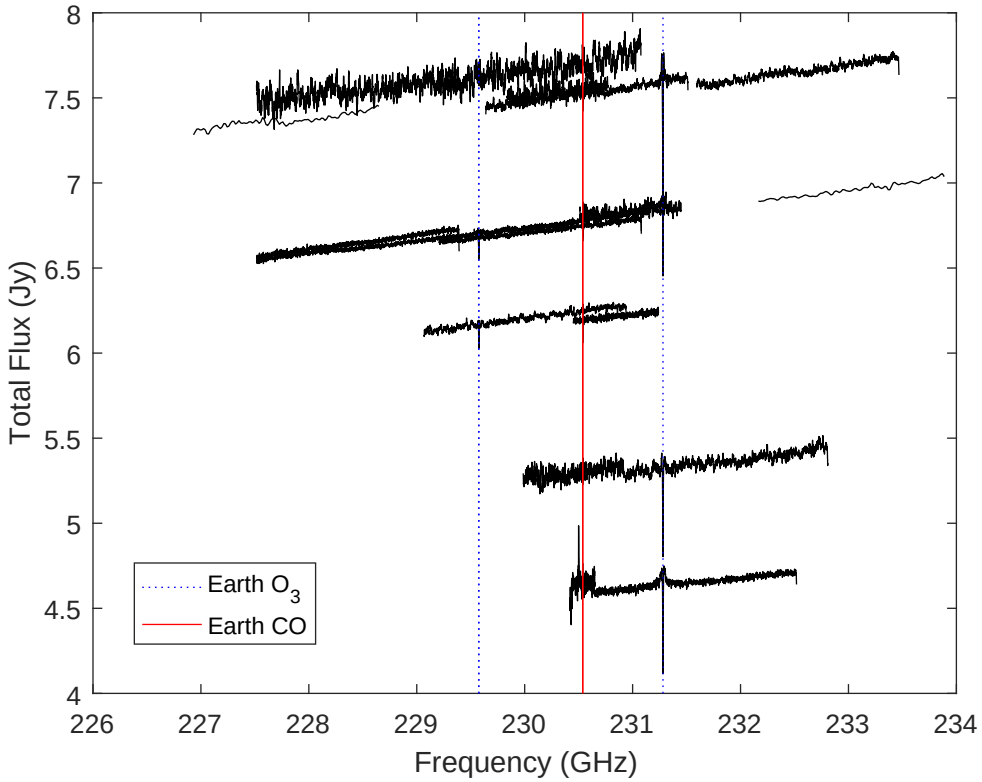

Figure 4.11: All spectra in TOPO mode in which the red line marks the position of $CO_{J=2-1}$ transition in the Earth's atmosphere and the dotted blue lines marks atmospheric O_3.

Figure 4.11 shows all spectra in TOPO mode in one plot. Since the position of CO in Callisto's atmosphere differs for each project, it is not shown. Instead, the position of $CO_{J=2-1}$ transition in the Earth's atmosphere by a red line and atmospheric O_3 by blue lines are demonstrated.

4.4 Average spectra

Since the point of this project is to constrain the CO content in Callisto's atmosphere, extracting an average spectrum is required. As it has been illustrated in previous section, none of the individual spectra has shown an obvious CO transition line in the atmosphere of Callisto. But still, it can be assumed that all spectra contain the same CO signal concealed in the noise. According to the mentioned radiometer equation in relation (1.3), increasing the integration time of observation leads to the reduction of rms noise. Integration time of the average spectrum is the sum of all integration times which have been spent for each spectrum. It means, averaging leads to increase intergration time and it consequently reduces the rms noise and may cause the appearance of CO line.
The flagging region is chosen ± 4MHz around the atmospheric CO and O_3 lines and flagged spectra are shown in Appendix C. The flagging region must cover at least the width of the lines to remove all data of the Earth's atmosphere. Afterwards all spectra are flagged, they are realigned in Callisto's rest frame and then averaging is performed.
The integrated brightness temperature is needed to calculate molecular column density. Therefore, it is more convenient to plot the average spectra in terms of brightness temperature. Since the distance of Callisto from the Earth differs for each observation, observed flux densities of each spectrum must be converted to brightness temperature by using relations (2.24-2.26), before averaging.
Averaging of the functions or data sets is possible only if they have the same values on the x-axis. Then, the averaging can be performed over the values of y-axis. In mathematics, interpolation is a method to construct new data points and this is performed by Interp1 command in Matlab. Since the extracted spectra have no common frequency values at all, a frequency channel which is common in all spectra must be selected as a reference for x-axis. Then, Interp1 produces new values of flux (y-axis) associated with the reference frequencies. The averaging of spectra is performed for both hemispheres of Callisto in the interval of $CO_{J=2-1}$ transition frequency.
Figure 4.12 illustrates the average spectrum of trailing hemisphere of Callisto in terms of brightness temperature with approximately 0.20 K derived rms noise and 712 s ($\sim$ 12 min) total integration time. This spectrum is shown in figure 4.13 again while it has been zoomed and linearly fitted, with a green line which marks $CO_{J=2-1}$ transition in Callisto's atmosphere.
Figure 4.14 shows the average spectrum of leading hemisphere of Callisto in terms of brightness temperature as well, with approximately 0.14 K extracted rms noise and 569 s ($\sim$10 min) total integration time. This spectrum is shown again in figure 4.15 while it has been zoomed and linearly fitted, with a green line which denotes $CO_{J=2-1}$ transition in Callisto's atmosphere.
Considering both average spectra reveals apparently there is not an obvious transition line for CO, neither in trailing hemisphere nor the leading side. But still calculation of upper column density of CO in the atmosphere of Callisto is possible

which will be explained in the next chapter.

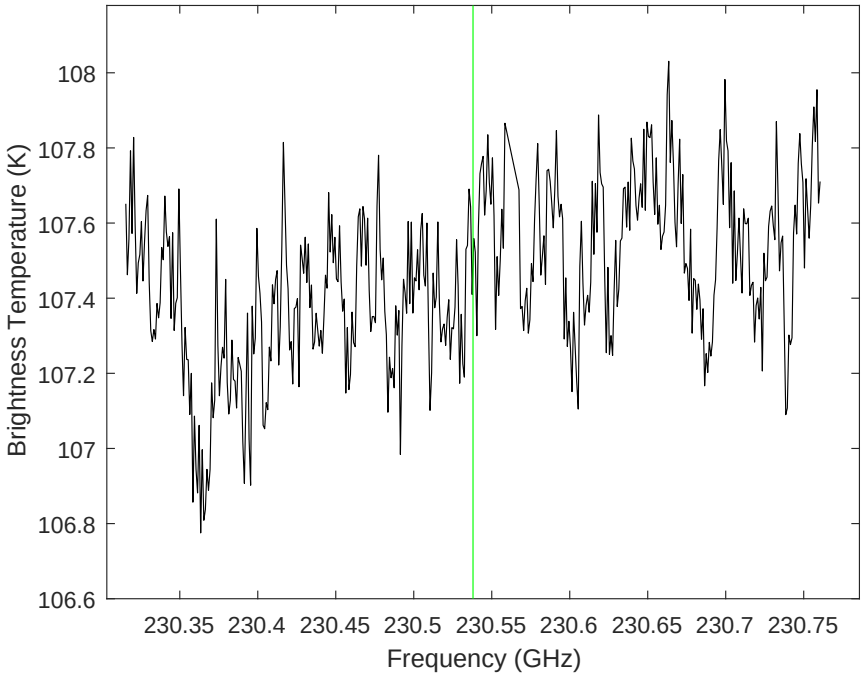

Figure 4.12: The average spectrum of trailing hemisphere, in Callisto's rest frame in which the green line denotes $CO_{J=2-1}$ transition in Callisto's atmosphere (ν = 230.538 GHz) with derived 0.1994 K rms noise.

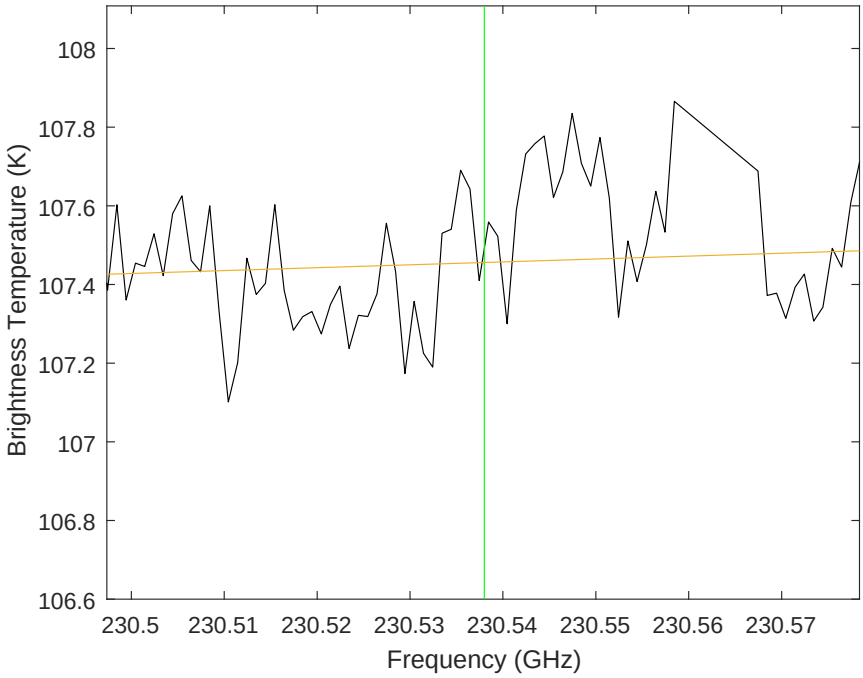

Figure 4.13: The fitted average spectrum of trailing hemisphere, in Callisto's rest frame in which the green line marks $CO_{J=2-1}$ transition in Callisto's atmosphere.

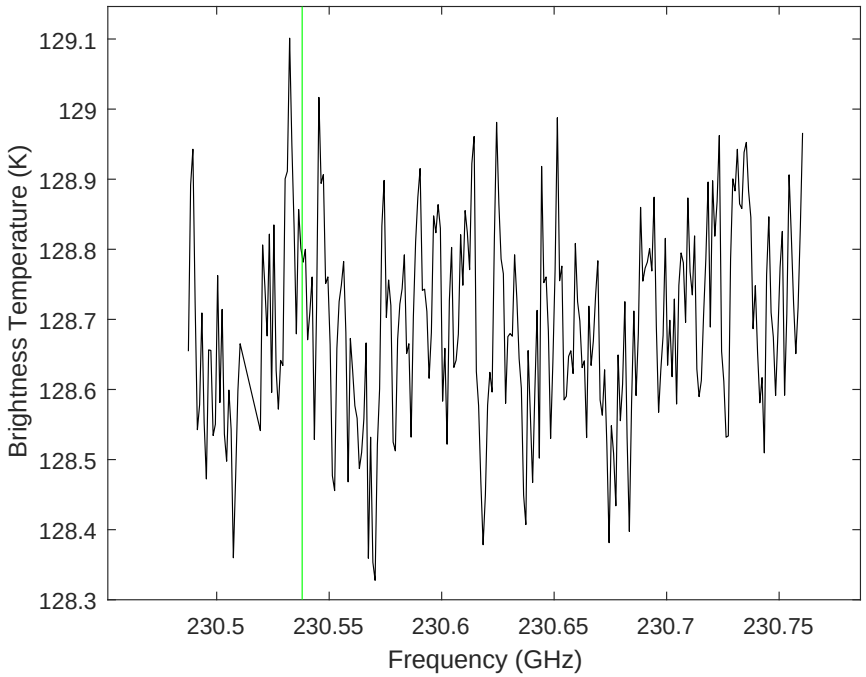

Figure 4.14: The average spectrum of leading hemisphere, in Callisto's rest frame in which the green line denotes $CO_{J=2-1}$ transition in Callisto's atmosphere (ν = 230.538 GHz) with derived 0.1389 K rms noise.

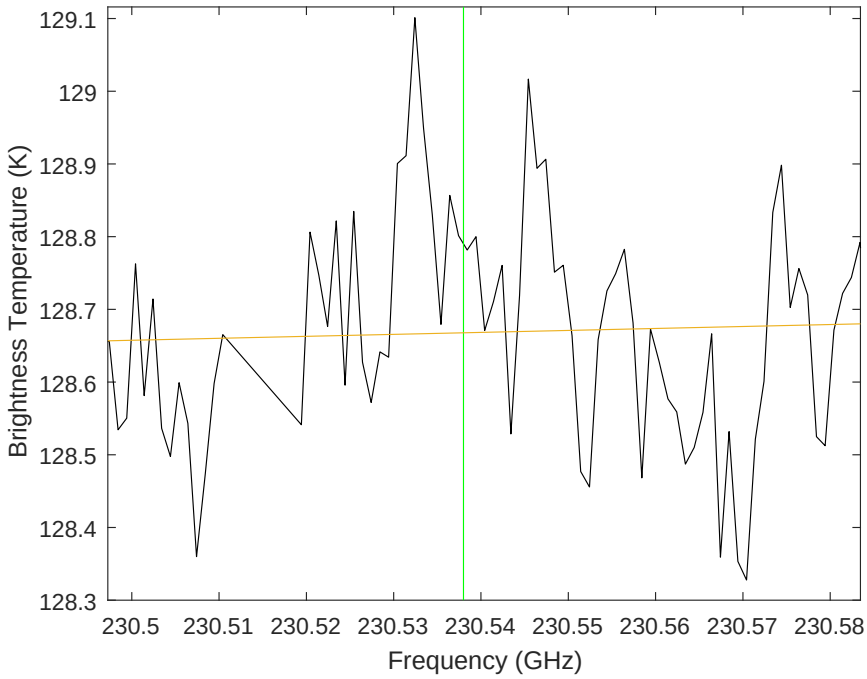

Figure 4.15: The fitted average spectrum of leading hemisphere, in Callisto's rest frame in which the green line marks $CO_{J=2-1}$ transition in Callisto's atmosphere.

5

Analysis and discussion

5.1 Spectral Analysis

Using the explained relations in the theory section gives the properties of illustrated spectra (section 4.3), which are presented in tables 5.1 and 5.2 :

Project ID/ Date	rms (mJy)	$\Delta\Omega$ (Sr)	Continuum Flux (Jy)	Continuum Temperature (K)	Observation time (s)
2012.1.00377.s (29-Jan-2014)	50	4.4×10^{-11}	7.67	107.3±0.1	143
2012.1.00640.s (03-Apr-2014)	33	3.0×10^{-11}	5.29	106.4±0.1	143
2012.1.00013.s (28-Apr-2014)	57	2.6×10^{-11}	4.64	107.0±0.1	143
2013.1.00862.s (11-Dec-2014)	11	2.9×10^{-11}	6.20	128.8±0.1	142
2012.1.00377.s (25-Dec-2014)	10	3.2×10^{-11}	6.75	129.3±0.1	142
2012.1.00377.s (28-Dec-2014)	12	3.3×10^{-11}	6.78	127.9±0.1	142
2013.1.00457.s (28-Dec-2014)	30	3.3×10^{-11}	6.82	128.5±0.1	142
2013.1.00319.s (29-Jan-2015)	33	4.3×10^{-11}	7.55	107.6±0.1	142
2013.1.00661.s (29-Jan-2015)	37	4.2×10^{-11}	7.52	107.9±0.1	142
2013.1.00773.s (04-Apr-2015)	14	3.5×10^{-11}	6.25	107.9±0.1	142

Table 5.1: General properties of all spectra

Table 5.1 presents some general properties of extracted spectra. Second column of the table shows the rms noise derived for each observation. The source of the noise for any observation could be the thermal noise of electronic devices or radio frequency interference. Third column illustrates the solid angle of Callisto so that, it has been assumed as a circular disk which has been observed from the surface of the Earth. The last three columns of the table 5.1 show flux of the spectrum, temperature of the spectrum and Callisto's observation time in second, respectively. Table 5.2 presents the details of the detected lines in the spectra. It illustrates the exact frequency of the appeared lines and the observed flux at the line center for

Project ID (Figure)	Observed line	line-Frequency (GHz)	line-Flux (Jy)	FWHM (km/s)	tau (τ)
2012.1.00640.s (Fig. **??**)	O_3	231.2816	4.80	7.39	0.10
2012.1.00013.s (Fig. 4.5)	O_3	231.2816	4.12	5.83	0.12
2012.1.00377.s (Fig. 4.9)	O_3	229.5745	6.55	4.05	0.03
	CO	230.5376	6.66	2.60	0.01
2012.1.00377.s (Fig. 4.11)	O_3	229.5745	6.58	4.83	0.03
	CO	230.5376	6.68	2.47	0.01
2013.1.00457.s (Fig. 4.13)	O_3	231.2816	6.45	3.26	0.05
2013.1.00661.s (Fig. 4.17)	O_3	231.2816	6.74	5.84	0.11
	CO	230.5376	7.42	2.60	0.01
2013.1.00773.s (Fig. 4.19)	O_3	229.5755	6.03	4.05	0.04
	CO	230.5376	6.06	2.47	0.03

Table 5.2: Properties of appeared lines in all spectra

each frequency. Based on the results, it can be concluded that the detected lines are come from the atmosphere of the Earth. It can be said that each project that possesses an absorption CO line, contains also atmospheric O_3, but this is not valid conversely. Measuring FWHM (Full width Half Maximum) of the lines which is a quantity to show how wide the detected lines are, eventuates atmospheric ozone lines are wider than monoxide carbon lines. Also, the width of CO lines are more or less constant, whereas O_3's are not. In the last column of the table 5.2, opacity is calculated that shows how the atmosphere of the Earth is opaque for the radiation at the specific frequency.

5.2 CO column density

In order to calculate an upper column density limit for CO, an upper limit on the integrated intensity has to be estimated, from the noise level and the expected line width (FWHM). Before going through the calculations, the velocity dispersion of CO molecules, by using theoretical relations and detected water lines will be calculated, to see how the velocity of CO molecules is distributed.
Maxwell-Boltzmann distribution is considered to obtain the velocity dispersion of the gas particles. This is valid if the gas which is CO would be an ideal gas and its particles move freely under a stationary circumstances, without interacting with each other. It implies that the system is experiencing a LTE in which, the molecules of CO are in equilibrium with the ambient gas. In this case, the excitation temperature of CO molecules (T_{ex}) equals the kinetic temperature (T_k) of the particles. According to the Maxwellian velocity distribution, the most likely speed that CO molecules possess, is given by:

$$v_p = \sqrt{\frac{2kT}{m}} \tag{5.1}$$

where k is the Boltzmann constant, T is the temperature of the ambient gas and m is

the mass of one CO molecule in kg. Using the relation $M = mN_A$ in which, M is the molar mass and N_A is the Avogadro constant, and derived brightness temperature of Callisto from SMA observer center (120 K), v_p is calculated as:

$$v_p = 266.89 \quad m/s \quad \simeq 0.3 \quad km/s \tag{5.2}$$

Therefore according to Maxwellian distribution, CO molecules must move with $v \sim$ 0.3 km/s on average.
Since it has been assumed that CO is experiencing LTE, it can be concluded that kinetic temperature of CO molecules are equivalent to the kinetic temperature of other species such as water molecules and all molecules are moving with the same speed. Thus, CO transition line must have a similar line width as water. Hence, by using the result of water detection from the atmosphere of Callisto (Hartogh et al.,2013), the FWHM of the detected line is derived directly from the spectra as:

$$FWHM_{water} = \Delta\nu = 2.5 \quad MHz \tag{5.3}$$

By using water rest frequency (556.936 GHz), this value can be converted to km/s as:

$$FWHM_{water} = \Delta v = 1.35 \quad km/s \tag{5.4}$$

The velocity of water line is much larger than the calculated velocity by Maxwellian distribution which implies there must be some additional movements in the atmosphere of Callisto (long distance movements).
Since no transition line is detected in the average spectra, it can be said that the line is optically thin and using the relation (2.38) will be appropriate in this case. The required quantities using in relation (2.38) is shown in the table 5.3:

Body Callisto	ν (GHz)	T_{ex} (K)	B GHz	g_u	E_u (K)	T_b (K)	Δv (km/s)
Leading	230.538	120	57.636	5	16.6	0.104	1.35
Trailing	"	"	"	"	"	0.149	"

Table 5.3: Required quantities to calculate CO upper column density. T_{ex} is the temperature of Callisto according to SMA observer center and E_u is the energy of upper state (Wilson et al.,2013). The peak brightness temperature (T_b) for leading and trailing sides is given by three times the rms noise.

The average spectra did not reveal any detectable line to be able to measure the peak brightness temperature. In this case, since the spectra should have a Gaussian distribution of noise, three times the rms noise level is chosen as the upper limit of the brightness temperature, to be conservative and assure that the probability for the signal being within this limit is 99.7%
Substituting calculated quantities of table 5.3 in relation (2.38), gives upper column density of CO for both hemispheres of Callisto:

$$N(CO)_{Leading} = 2.02 \times 10^{15} \quad cm^{-2} \tag{5.5}$$

And,

$$N(CO)_{Trailing} = 2.90 \times 10^{15} \quad cm^{-2} \tag{5.6}$$

The difference between calculated upper column densities of trailing and leading hemispheres of Callisto is mainly because of different noise levels in spectra which have been averaged over different total integration time.
Comparing the results of the average spectra with the measured column densities of detected CO_2 (9.2×10^{14} cm^{-2}) and O_2 ($\sim 4 \times 10^{15}$ cm^{-2}) which are mentioned in the introduction, shows that CO can not be the dominant molecule in the atmosphere of Callisto, though being the second major molecule is plausible.
Calculated upper limit of CO column density, suggests that we still might be able to detect CO in the atmosphere of Callisto. Reducing rms noise via increasing the integration time, will allow for CO lines to be detected if, it is more abundant than CO_2 in Callisto's atmosphere. In this case, according to the theoretical atmosphere model by Vorburger et al (2015), it could be inferred that the ice component of Callisto's surface was formed in oxidizing state which implies that the satellite has been accreted in proto-solar nebula[1] and it has been formed at the same time as its host giant planet.

5.3 Titan

To compare the extracted spectra of Callisto with corresponding data from a moon known to have a thick atmosphere, spectra of Titan from ALMA online archive was also extracted for this project.
In the method chapter, all steps to extract the data are explained and they all are the same for Titan. The data associated with the $CO_{J=3-2}$ transition has been searched and no available project was found in this case.
Figure 5.1 shows the spectra associated with $CO_{J=2-1}$ transition for Titan. These spectra, unlike the spectra of Callisto, contain very strong CO lines. Since these data have been collected during different periods of time, distance of Titan from the Earth varies in both spectra which leads to observe different flux densities. According to the relative motion of Titan produced by JPL ephemeris, in both cases Titan has been moving towards the Earth. Some general properties of spectra are shown in table 5.4.
To estimate the CO column density in Titan's atmosphere, almost the same quantities which are used for Callisto's atmosphere are needed. Titan has a temperature profile varying with altitude (De Pater and Lissauer,2015) and the lower limit of temperature is assumed as the excitation temperature (100 K).

[1]When a star is born, a flattened molecular clouds rotating around the central star is formed which is called proto-solar nebula or proto-planetary disc

Spectra	Distance (AU)	Δv (km/s)	Peak-flux (Jy)	Diameter (")
Figure 5.1, left panel	10.89	-8.45	2.5369	0.456 ± 0.008
Figure 5.1, right panel	9.07	-15.48	4.3649	0.817 ± 0.002

Table 5.4: Extracted properties of Titan's Spectra

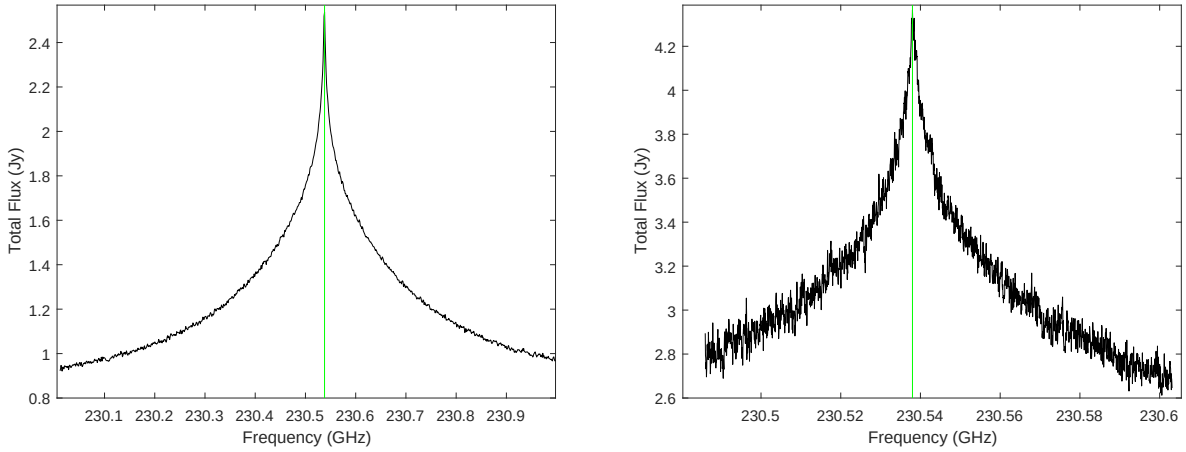

Figure 5.1: The Extracted spectra of Titan plotted in Titan's rest frame. The left panel is the spectrum of the project 2015.1.00513.s which has been observed in 27 Dec 2015, with 12.8 mJ rms noise. The right panel is the spectrum of the project 2013.1.00839.s which has been observed in 25 April 2015, with 42.4 mJ rms noise. The green line marks the position of CO (2-1) transition in Titan's atmosphere.

Titan is the only satellite in the Solar System which has a thick atmosphere and the detected broad CO lines with high peaks, is its confirmation. In this case, when the line shape is clearly non-Gaussian, the integrated brightness temperature is measured as the surface area under the line. The lines are so broad that they each cover the whole spectral window and the continuum level can not be directly measured. For the purpose of this exercise, the continuum is roughly estimated to be 1 Jy for the left spectrum in figure 5.1 and 2.8 Jy for the right spectrum in figure 5.1. The required quantities using in relation (2.38) are shown in table 5.5:

Body Titan	T_{ex} (K)	B GHz	g_u	E_u (K)	Integrated-T_b (K)
Figure 5.1, left spectrum	100	57.636	5	16.6	1.8×10^4
Figure 5.1, right spectrum	"	"	"	"	2.6×10^4

Table 5.5: Required quantities to estimate CO column density in the atmosphere of Titan.

Since the detected lines in Titan's spectra are thick, it is hard to estimate their

optical depth. Thus, as a rough estimate, the relation (2.38) is used to calculate the lower limit of CO in Titan's atmosphere and then, by using relation (2.39), total column density of CO will be estimated for assumed optical depths. The results are derived as:

Spectra	$N_{tot}(CO)(cm^{-2})$ $\tau << 1$	$N_{tot}(CO)(cm^{-2})$ $\tau = 1$	$N_{tot}(CO)(cm^{-2})$ $\tau = 5$
Figure 5.1, left spectrum	2.6×10^{20}	4.1×10^{20}	13.0×10^{20}
Figure 5.1, right spectrum	3.7×10^{20}	5.8×10^{20}	18.6×10^{20}

Table 5.6: Estimated CO column density in the atmosphere of Titan by using ALMA online archival data.

The calculated results in the table 5.6 due to the used assumption for lower limit of excitation temperature, subtracted baselines and approximated optical depth are considered as the lower limit ($\tau << 1$) and estimation of CO column density in Titan's atmosphere, for the given optical depths. Comparing the calculated column densities of CO and CH_2CHCN ($3.7 \times 10^{13} - 1.4 \times 10^{14}$ cm^{-2}) implies that, Titan has a rich atmosphere of CO.

6

Conclusion

The detection of CO_2 in the atmosphere of Callisto, in combination with predictions from theoretical models of Callisto's atmosphere, motivated a search for $CO_{J=2-1}$ transition lines in the extracted spectra of ALMA archival data associated with Callisto.

To be able to fit the extracted visibilities, we assumed Callisto as a circular disc. Then, Fourier transform of intensity distribution of assumed model was compared to the observed visibilities and the best fitted total fluxes were derived. The resulting ten spectra covering the $CO_{J=2-1}$ transition, are from the period of January 2014 to April 2015.

To reduce the rms noise level, an average spectrum was extracted separately for the leading and trailing hemispheres of Callisto. Before averaging, Earth atmospheric CO and O_3 lines, which were detected in some spectra, were flagged to avoid contamination in the final rms noise level.

Comparing calculated upper column densities of CO for both leading (2.02×10^{15} cm^{-2}) and trailing (2.90×10^{15} cm^{-2}) sides, with those reported for CO_2 ((9.2×10^{14} cm^{-2}) and O_2 ($\sim 4 \times 10^{15}$ cm^{-2}) implies that, although CO is not the dominant molecule in the atmosphere of Callisto, it still could be the second major species. Upper column density of CO is quite large enough to be optimistic about detecting CO lines directly. Increasing total integration time will cause reduction in rms noise level which consequently may cause CO line to be detectable. So if CO lines could be detected, based on theoretical atmosphere model of Callisto, it can be concluded that Callisto's atmosphere, with an icy surface, has been formed in oxidizing state in proto-solar nebula.

CO column density in the atmosphere of Titan is estimated for three different optical depths. Comparing upper limits of CO in the atmosphere of Callisto and estimated CO column density in Titan's atmosphere shows that, Titan's atmosphere is $\sim 10^5$ times denser in CO than in that of Callisto, which is an obvious confirmation of Titan's thick atmosphere.

The extracted ground based data from Callisto could be used to preparation for ESA's JUICE mission which is planned to be launched in 2022 and arrived at Jupiter's system in 2030, to observe Jupiter and its three largest moons Ganymede, Callisto and Europa, in more details.

A

Extracted Spectra

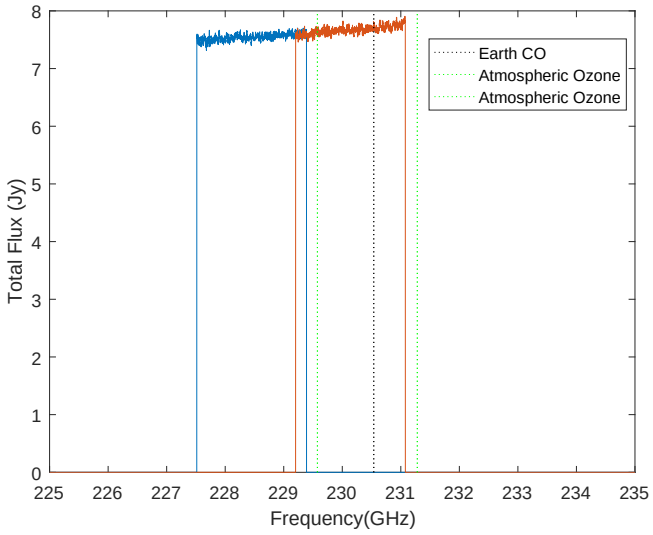

Figure A.1: The spectrum of the project 2012.1.00377.s which has been observed in 29th January 2014.

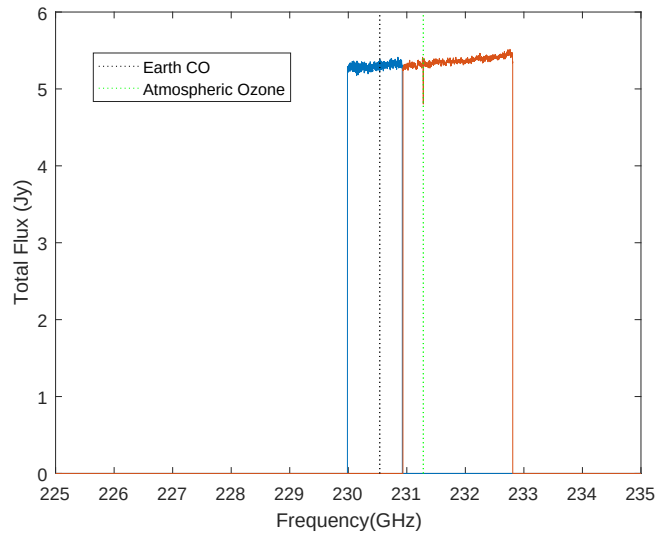

Figure A.2: The spectrum of the project 2012.1.00640.s

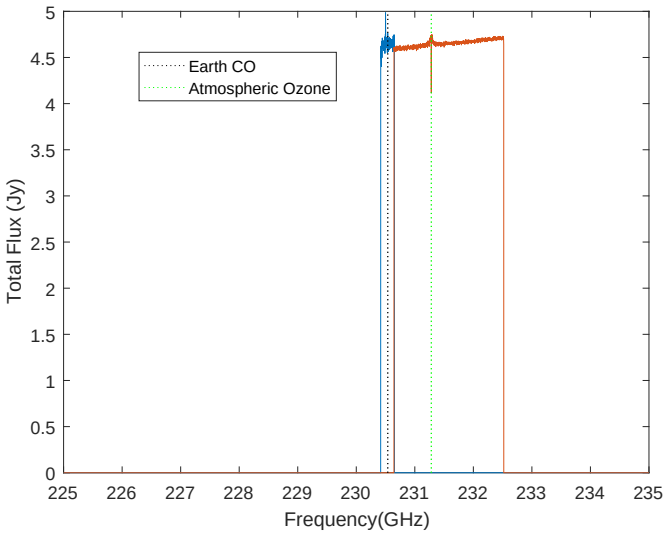

Figure A.3: The spectrum of the project 2012.1.00013.s

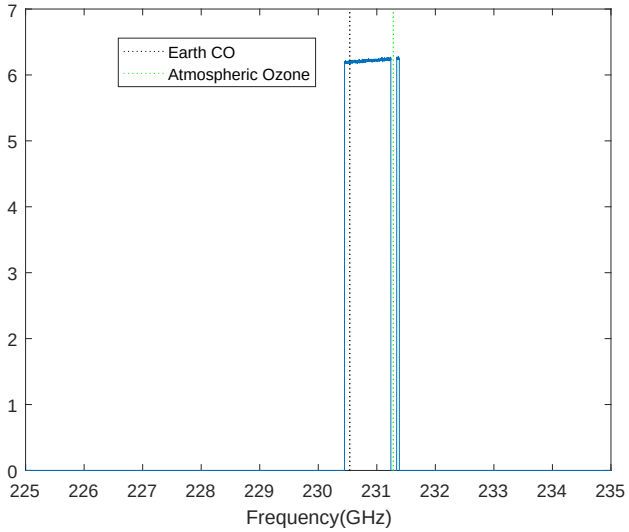

Figure A.4: The spectrum of the project 2013.1.00862.s

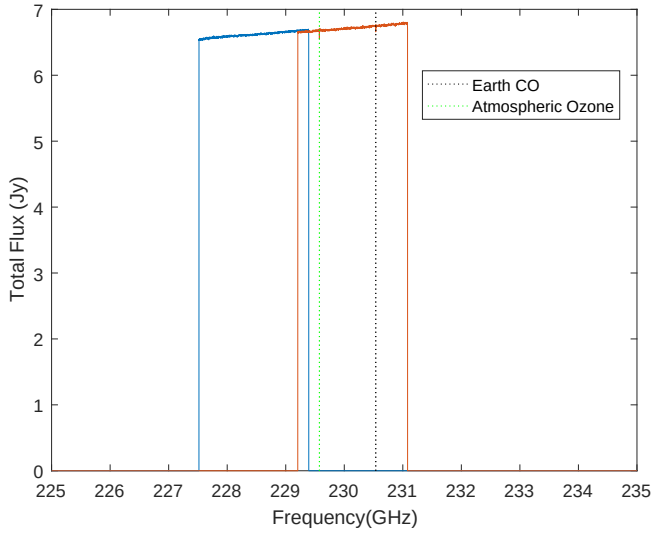

Figure A.5: The spectrum of the project 2012.1.00377.s which has been observed in 25th December 2014.

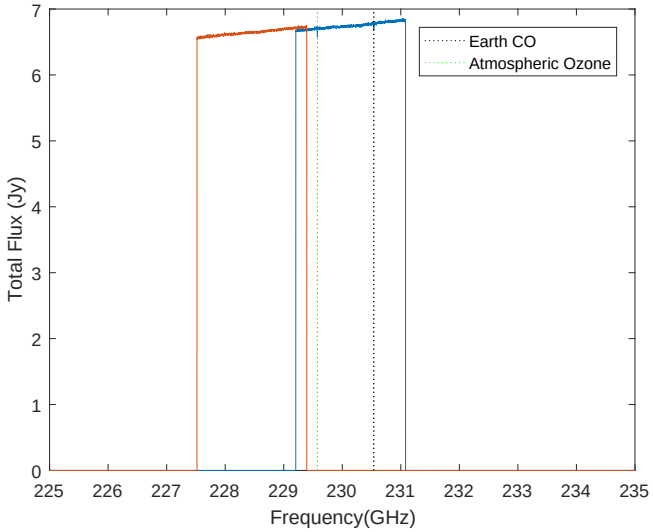

Figure A.6: The spectrum of the project 2012.1.00377.s which has been observed in 28*th* December 2014.

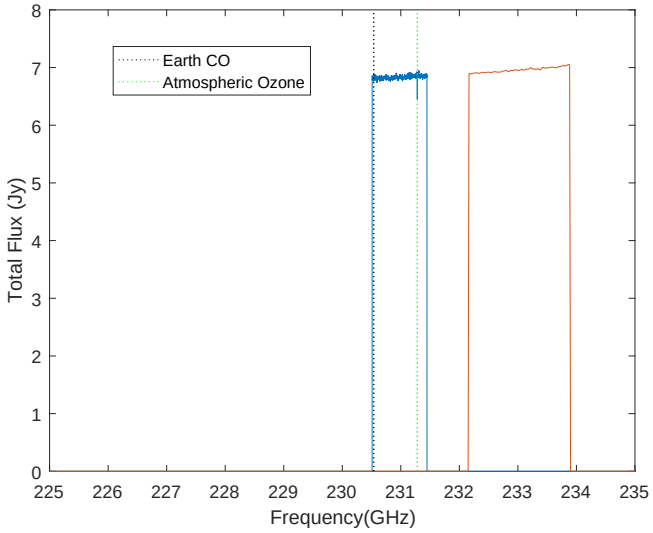

Figure A.7: The spectrum of the project 2013.1.00457.s

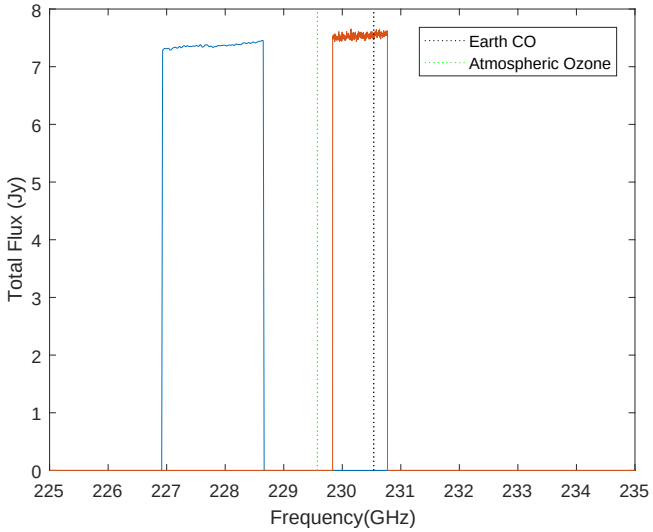

Figure A.8: The spectrum of the project 2013.1.00319.s

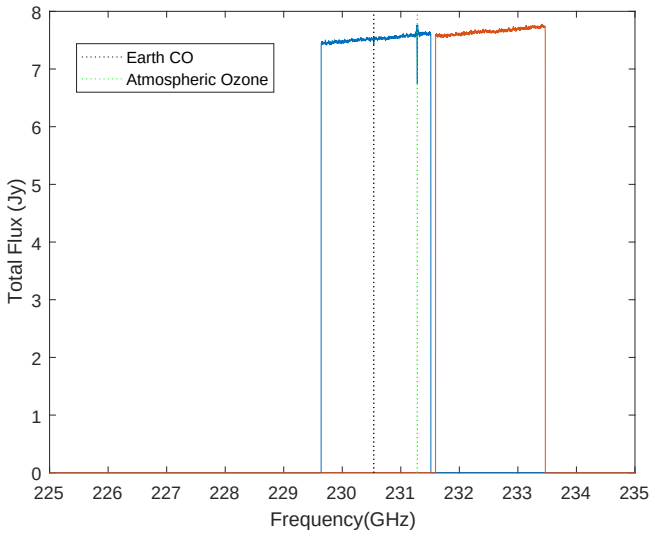

Figure A.9: The spectrum of the project 2013.1.00661.s

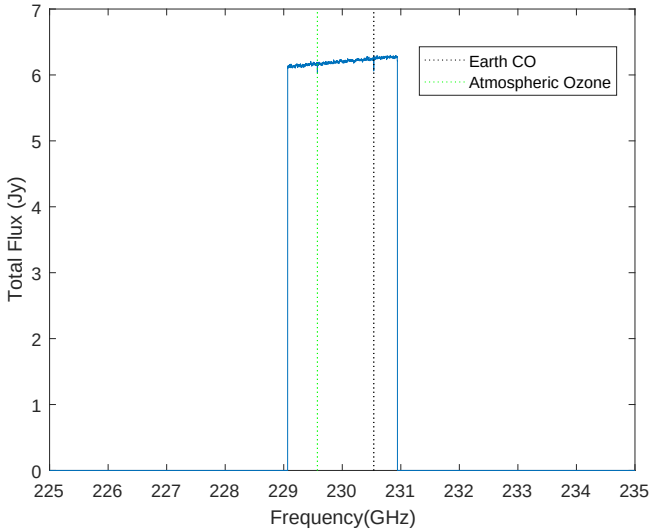

Figure A.10: The spectrum of the project 2013.1.00773.s

B

Atmospheric ozone spectral lines

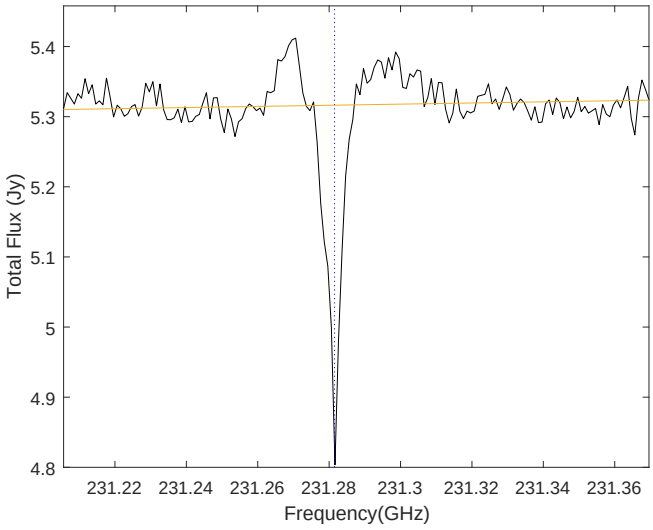

Figure B.1: The spectrum of the project 2012.1.00640.s which includes the line of atmospheric ozone at 231.28151 GHz.

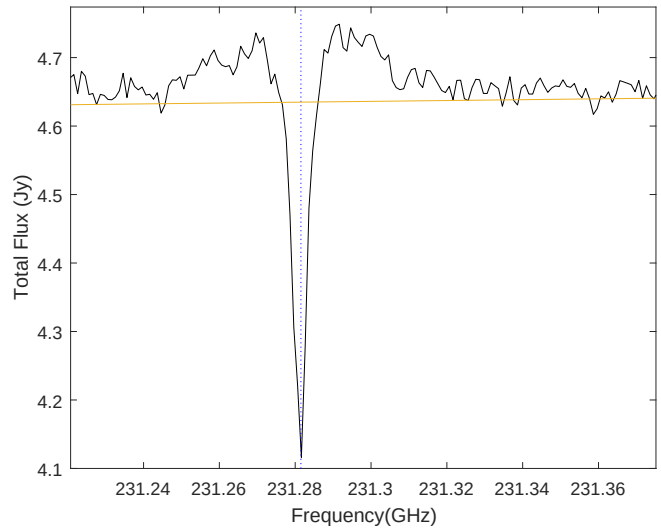

Figure B.2: The spectrum of the project 2012.1.00013.s which includes the line of atmospheric ozone at 231.28151 GHz.

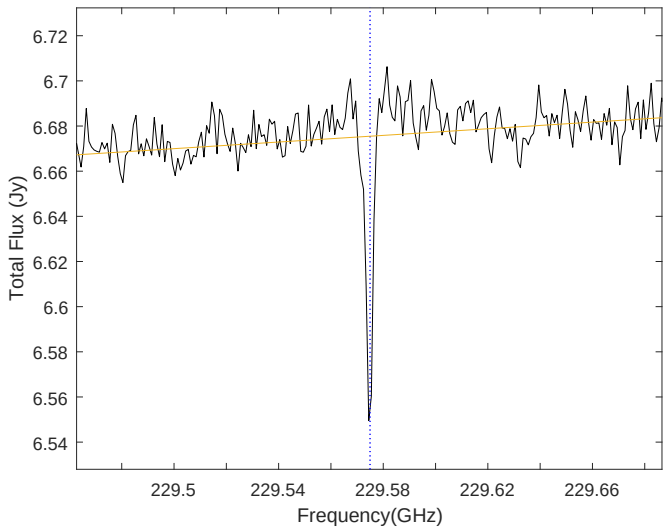

Figure B.3: The spectrum of the project 2012.1.00377.s which is observed in 25-Dec-2014 and includes the line of atmospheric ozone at 229.57495 GHz.

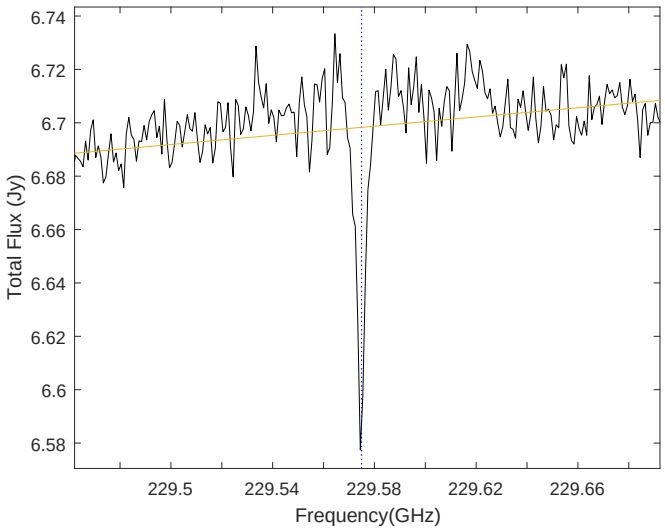

Figure B.4: The spectrum of the project 012.1.00377.s which is observed in 28-Dec-2014 and includes the line of atmospheric ozone at 231.28151 GHz.

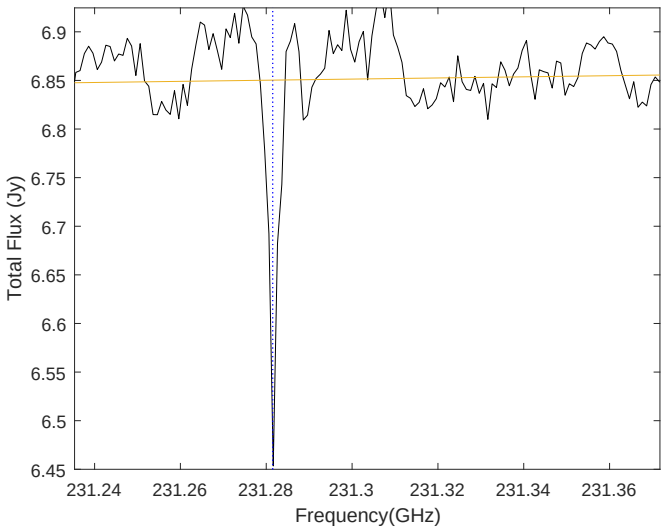

Figure B.5: The spectrum of the project 2013.1.00457.s which includes the line of atmospheric ozone at 231.28151 GHz.

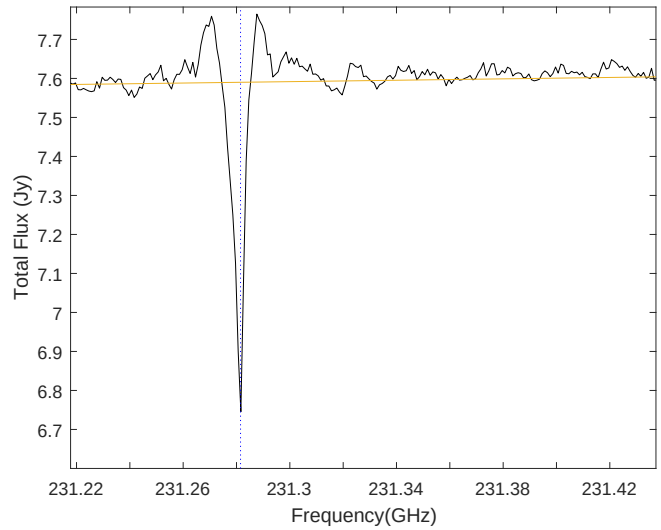

Figure B.6: The spectrum of the project 2013.1.00661.s which includes the line of atmospheric ozone at 231.28151 GHz.

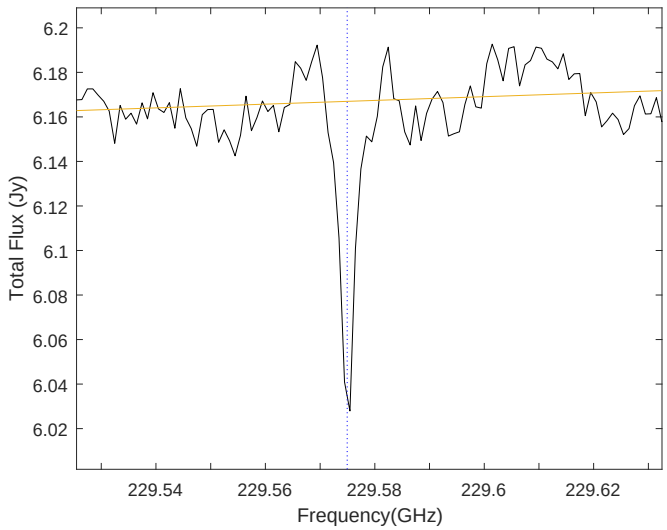

Figure B.7: The spectrum of the project 2013.1.00773.s which includes the line of atmospheric ozone at 229.57495 GHz.

C

Flagged spectra

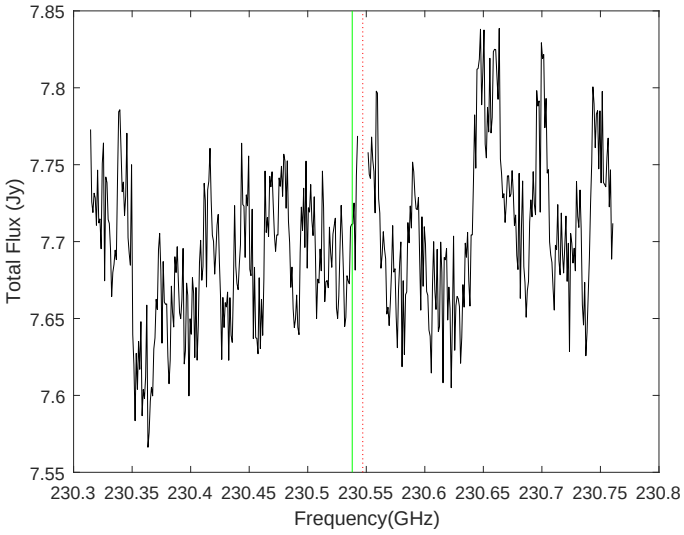

Figure C.1: The spectrum of the project 2012.1.00377.s (Obs:29-Jan-2014) in which, the Earth atmospheric CO line (red dashed line) is flagged. The green line marks the position of CO (2-1) transition in the atmosphere of Callisto ($\nu = 230.538$ GHz).

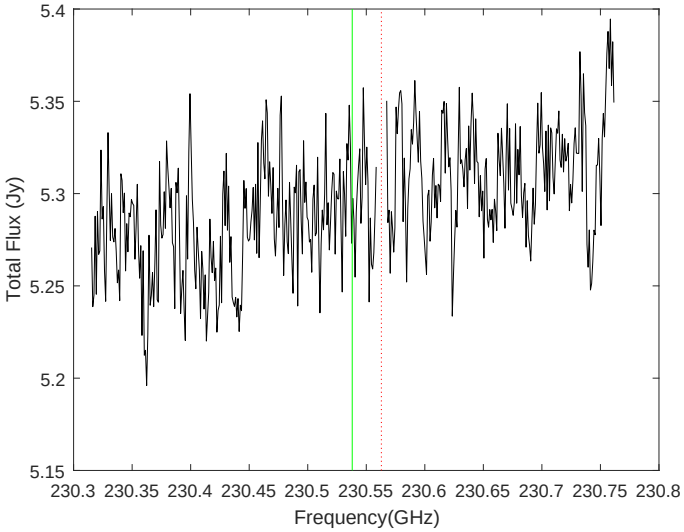

Figure C.2: The spectrum of the project 2012.1.00640.s in which, the Earth atmospheric CO line (red dashed line) is flagged. The green line marks the position of CO (2-1) transition in the atmosphere of Callisto ($\nu = 230.538$ GHz).

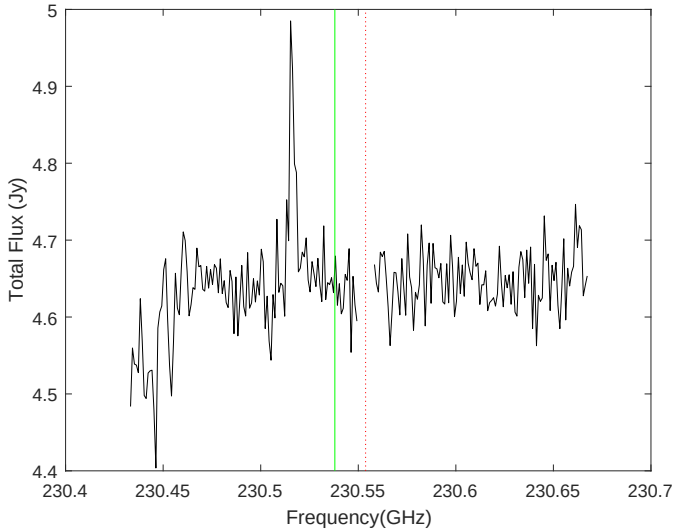

Figure C.3: The spectrum of the project 2012.1.00013.s in which, the Earth atmospheric CO line (red dashed line) is flagged. The green line marks the position of CO (2-1) transition in the atmosphere of Callisto ($\nu = 230.538$ GHz).

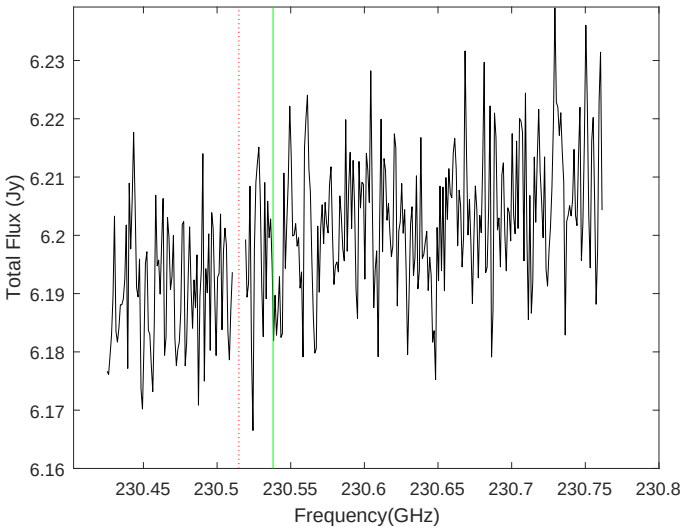

Figure C.4: The spectrum of the project 2013.1.00862.s in which, the Earth atmospheric CO line (red dashed line) is flagged. The green line marks the position of CO (2-1) transition in the atmosphere of Callisto ($\nu = 230.538$ GHz).

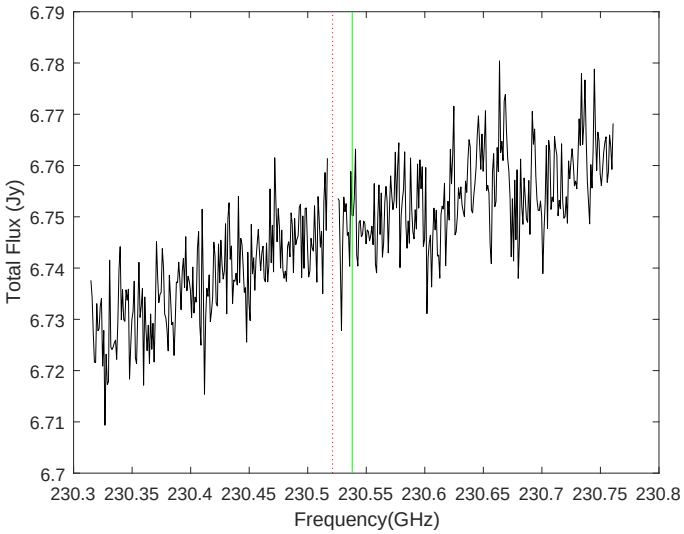

Figure C.5: The spectrum of the project 2012.1.00377.s (Obs:25-Dec-2014) in which, the Earth atmospheric CO line (red dashed line) is flagged. The green line marks the position of CO (2-1) transition in the atmosphere of Callisto ($\nu = 230.538$ GHz).

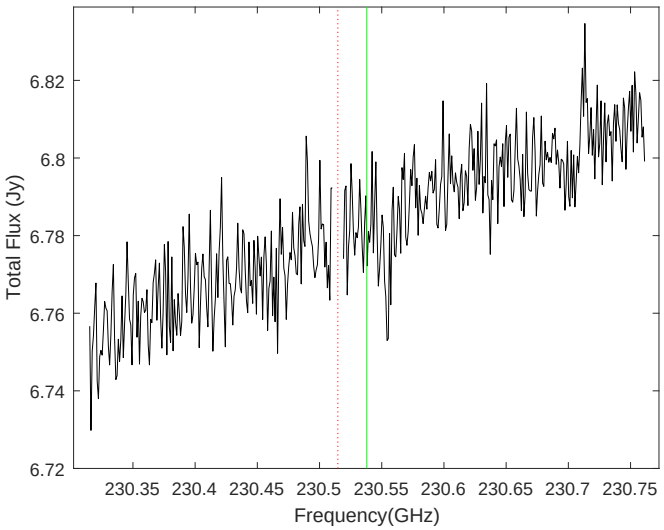

Figure C.6: The spectrum of the project 2012.1.00377.s (Obs:28-Dec-2014) in which, the Earth atmospheric CO line (red dashed line) is flagged. The green line marks the position of CO (2-1) transition in the atmosphere of Callisto ($\nu = 230.538$ GHz).

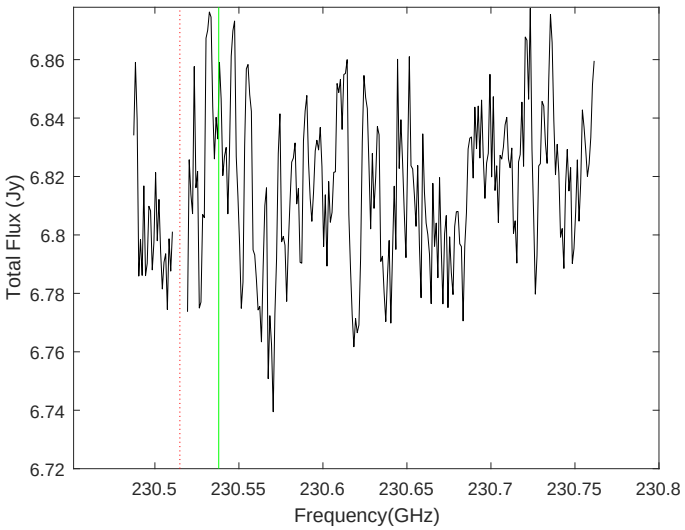

Figure C.7: The spectrum of the project 2013.1.00457.s in which, the Earth atmospheric CO line (red dashed line) is flagged. The green line marks the position of CO (2-1) transition in the atmosphere of Callisto ($\nu = 230.538$ GHz).

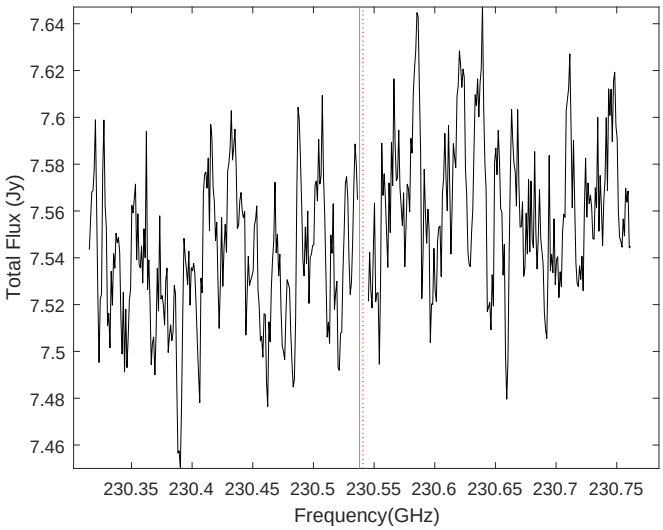

Figure C.8: The spectrum of the project 2013.1.00319.s in which, the Earth atmospheric CO line (red dashed line) is flagged. The green line marks the position of CO (2-1) transition in the atmosphere of Callisto ($\nu = 230.538$ GHz).

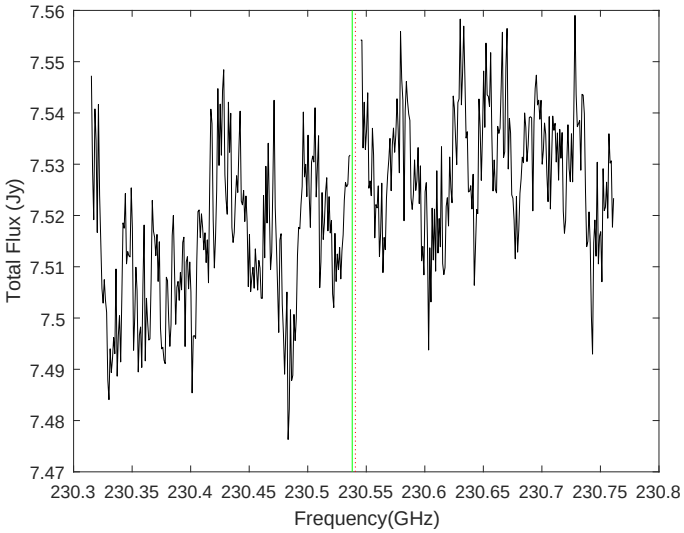

Figure C.9: The spectrum of the project 2013.1.00661.s in which, the Earth atmospheric CO line (red dashed line) is flagged. The green line marks the position of CO (2-1) transition in the atmosphere of Callisto ($\nu = 230.538$ GHz).

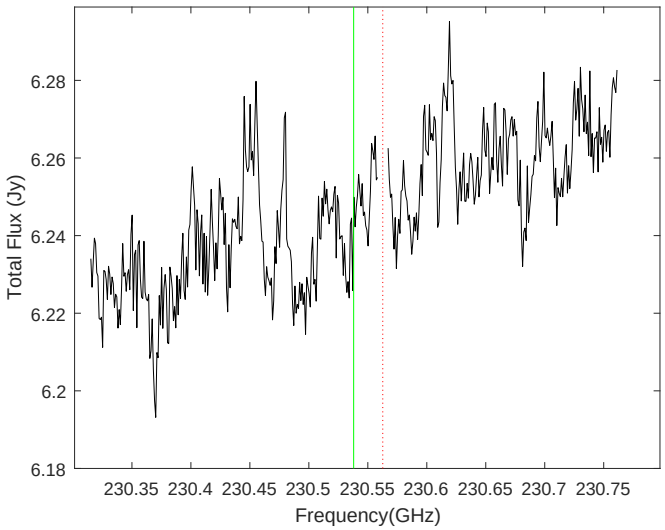

Figure C.10: The spectrum of the project 2013.1.00773.s in which, the Earth atmospheric CO line (red dashed line) is flagged. The green line marks the position of CO (2-1) transition in the atmosphere of Callisto ($\nu = 230.538$ GHz).

Bibliography

ALMA-Observatory. Almaobservatory, 2017. URL http://www.almaobservatory.org/en/home/.

JD Anderson, RA Jacobson, TP McElrath, WB Moore, G Schubert, and PC Thomas. Shape, mean radius, gravity field, and interior structure of Callisto. *Icarus*, 153(1):157–161, 2001.

Robin M Canup and William R Ward. Formation of the Galilean satellites: Conditions of accretion. *The Astronomical Journal*, 124(6):3404, 2002.

Robert W Carlson. A tenuous carbon dioxide atmosphere on Jupiter's moon Callisto. *Science*, 283(5403):820–821, 1999.

Arnab Rai Choudhuri. *Astrophysics for physicists*. Cambridge University Press, 2014.

Athena Coustenis and Mathieu Hirtzig. Cassini–Huygens results on Titan's surface. *Research in Astronomy and Astrophysics*, 9(3):249, 2009.

Nathaniel J Cunningham, John R Spencer, Paul D Feldman, Darrell F Strobel, Kevin France, and Steven N Osterman. Detection of Callisto's oxygen atmosphere with the Hubble Space Telescope. *Icarus*, 254:178–189, 2015.

Imke De Pater and Jack J Lissauer. *Planetary sciences*. Cambridge University Press, 2015.

AD Fortes. Exobiological implications of a possible ammonia–water ocean inside Titan. *Icarus*, 146(2):444–452, 2000.

Paul F Goldsmith and William D Langer. Population diagram analysis of molecular line emission. *The Astrophysical Journal*, 517(1):209, 1999.

Paul Hartogh, Dominique Bockelée-Morvan, Ladi Rezac, Raphael Moreno, Emmanuel Lellouch, Miriam Rengel, and Christopher Jarchow. *Detection and Characterization of Ganymede's and Callisto's Water Atmospheres*. Max Planck Institute for Solar System Research, Oct 2013. URL http://herschel.esac.esa.int/TheUniverseExploredByHerschel/presentations/13a-1720_HartoghP.pdf.

KK Khurana, MG Kivelson, DJ Stevenson, G Schubert, CT Russell, RJ Walker, and C Polanskey. Induced magnetic fields as evidence for subsurface oceans in Europa and Callisto. *Nature*, 395(6704):777–780, 1998.

AJ Kliore, A Anabtawi, RG Herrera, SW Asmar, AF Nagy, DP Hinson, and FM Flasar. Ionosphere of Callisto from Galileo radio occultation observations. *J. Geophys. Res*, 107(1407):10–1029, 2002.

Mao-Chang Liang, Benjamin F Lane, Robert T Pappalardo, Mark Allen, and Yuk L Yung. Atmosphere of Callisto. *Journal of Geophysical Research: Planets*, 110(E2), 2005.

Jeffrey G Mangum and Yancy L Shirley. How to calculate molecular column density. *Publications of the Astronomical Society of the Pacific*, 127(949):266, 2015.

Karl L Mitchell, Martin B Barmatz, Corey S Jamieson, Ralph D Lorenz, and Jonathan I Lunine. Laboratory measurements of cryogenic liquid alkane microwave absorptivity and implications for the composition of Ligeia Mare, Titan. *Geophysical Research Letters*, 42(5):1340–1345, 2015.

Giuseppe Mitri, Rachele Meriggiola, Alex Hayes, Axel Lefevre, Gabriel Tobie, Antonio Genova, Jonathan I Lunine, and Howard Zebker. Shape, topography, gravity anomalies and tidal deformation of Titan. *Icarus*, 236:169–177, 2014.

Jeffrey M Moore, Clark R Chapman, Edward B Bierhaus, Ronald Greeley, Frank C Chuang, James Klemaszewski, Roger N Clark, J Brad Dalton, Charles A Hibbitts, Paul M Schenk, et al. Callisto. *Jupiter. The planet, satellites and magnetosphere*, 1:397–426, 2004.

Susanna Musotto, Ferenc Varadi, William Moore, and Gerald Schubert. Numerical simulations of the orbits of the Galilean satellites. *Icarus*, 159(2):500–504, 2002.

K Nagel, D Breuer, and T Spohn. A model for the interior structure, evolution, and differentiation of Callisto. *Icarus*, 169(2):402–412, 2004.

NASA. Titan temperature lag maps animation, 2017a. URL https://www.nasa.gov/image-feature/jpl/pia20020/titan-temperature-lag-maps-animation.

NASA. NASA Solar System exploration, Callisto - in depth, 2017b. URL https://solarsystem.nasa.gov/planets/callisto/indepth.

JPL NASA. Molecular spectroscopy, Jet Propulsion Laboratory, 2017c. URL https://spec.jpl.nasa.gov/ftp/pub/catalog/catdir.html.

JPL NASA. Cassini-Huygens: News-features-the story of Saturn, 2017d. URL https://web.archive.org/web/20051202030828/http://saturn.jpl.nasa.gov/news/features/saturn-story/moons.cfm.

European Southern Observatory. ALMA - Atacama Large Millimeter/submillimeter Array, 2017. URL http://www.eso.org/public/teles-instr/alma/.

Maureen Y Palmer, Martin A Cordiner, Conor A Nixon, Steven B Charnley, Nicholas A Teanby, Zbigniew Kisiel, Patrick GJ Irwin, and Michael J Mumma. ALMA detection and astrobiological potential of vinyl cyanide on Titan. *Science Advances*, 3(7):e1700022, 2017.

TG Phillips, KB Jefferts, and PG Wannier. Observation of the j= 2 to j= 1 transition of interstellar CO at 1.3 millimeters. *The Astrophysical Journal*, 186:L19, 1973.

François Raulin and Tobias Owen. Organic chemistry and exobiology on Titan. In *The Cassini-Huygens Mission*, pages 377–394. Springer, 2003.

Joe Rosen and Lisa Quinn Gothard. *Encyclopedia of Physical Science (Facts on File Science Library), Volume 1 & 2*. Facts on File, 2010.

Adam P Showman and Renu Malhotra. The Galilean satellites. *Science*, 286(5437): 77–84, 1999.

SMA-ObserverCenter. Sma observer center:planetary visibility function calculator, 2017. URL http://sma1.sma.hawaii.edu/planetvis.html.

F Sohl. The interior structure of Ganymede and Callisto: Implications from gravity data. In *European Planetary Science Congress 2009*, page 785, 2009.

James Stevenson, Jonathan Lunine, and Paulette Clancy. Membrane alternatives in worlds without oxygen: Creation of an azotosome. *Science advances*, 1(1): e1400067, 2015.

Darrell F Strobel, Joachim Saur, Paul D Feldman, and Melissa A McGrath. Hubble Space Telescope imaging spectrograph search for an atmosphere on Callisto: A Jovian unipolar inductor. *The Astrophysical Journal Letters*, 581(1):L51, 2002.

Audrey Vorburger, Peter Wurz, H Lammer, S Barabash, and O Mousis. Monte-Carlo simulation of Callisto's exosphere. *Icarus*, 262:14–29, 2015.

FC Wasiak, D Androes, DG Blackburn, JA Tullis, J Dixon, and VF Chevrier. A geological characterization of Ligeia Mare in the northern polar region of Titan. *Planetary and Space Science*, 84:141–147, 2013.

JPL Horizons Web-Interface. Horizons web-interface, 2017. URL https://ssd.jpl.nasa.gov/horizons.cgi.

Thomas Wilson, Kristen Rohlfs, and Susanne Huettemeister. *Tools of Radio Astronomy*. Springer Berlin, 2013.

Christophe Zimmer, Krishan K Khurana, and Margaret G Kivelson. Subsurface oceans on Europa and Callisto: Constraints from Galileo magnetometer observations. *Icarus*, 147(2):329–347, 2000.